8-15-2014

Asymmetric Temporal Interactions of Sound-Evoked Excitatory and Inhibitory Inputs in the Mouse Auditory Midbrain

Munenori Ono
University of Connecticut School of Medicine and Dentistry

Douglas L. Oliver
University of Connecticut School of Medicine and Dentistry

JPn Neuroscience

The Journal of Physiology

J Physiol 592.16 (2014) pp 3647–3669

Asymmetric temporal interactions of sound-evoked excitatory and inhibitory inputs in the mouse auditory midbrain

Munenori Ono and Douglas L. Oliver

Department of Neuroscience, University of Connecticut Health Center, Farmington, CT 06030-3401, USA

Key points

- The temporal coding of sound is critical for the auditory system.
- Little is known about how sound evokes the timing of synaptic currents at higher levels of the auditory system and how the integration of these currents results in neural firing.
- In the inferior colliculus, excitatory and inhibitory synaptic currents evoked by long-duration sounds have different temporal properties with excitatory currents more variable than inhibitory currents.
- Within a neuron, the sequence of synaptic events suggests the fastest sound-evoked excitatory postsynaptic current (EPSCs) usually followed the inhibitory postsynaptic currents (IPSCs), and the slowest EPSCs preceded by IPSCs.
- Knowledge about the timing of neural activity in the midbrain is important for understanding how temporally complex sounds such as speech are processed and communicated to higher centres of the system.

Abstract In the auditory midbrain, synaptic mechanisms responsible for the precise temporal coding of inputs in the brainstem are absent. Instead, in the inferior colliculus (IC), the diverse temporal firing patterns must be coded by other synaptic mechanisms, about which little is known. Here, we demonstrate the temporal characteristics of sound-evoked excitatory and inhibitory postsynaptic currents (seEPSCs and seIPSCs, respectively) *in vivo* in response to long-duration tones. The seEPSCs and seIPSCs differ in the variability of their temporal properties. The seEPSCs have either early or late current peaks, and the early-peaked currents may be either transient or sustained varieties. The seIPSCs have only early-peaked sustained responses but often have offset responses. When measured in a single neuron, the seIPSC peaks usually follow early, transient seEPSCs, but the seIPSCs precede latest-peaking seEPSCs. A model of the firing produced by the integration of asymmetric seEPSCs and seIPSCs showed that the temporal pattern of the early-peaked sustained neurons was easily modified by changing the parameters of the seIPSC. These results suggest that the considerable variability in the peak time and duration of the seEPSCs shapes the overall time course of firing and often precedes or follows the less variable seIPSC. Despite this, the inhibitory currents are potent in modifying the firing patterns, and the inhibitory response to sound offset appears to be one area where the integration of excitatory and inhibitory synaptic currents is lacking. Thus, the integration of sound-evoked activity in the IC often employs the asymmetric temporal interaction of excitatory and inhibitory synaptic currents to shape the firing pattern of the neuron.

DOI: 10.1113/jphysiol.2014.275446

(Received 3 April 2014; accepted after revision 10 June 2014; first published online 20 June 2014)
Corresponding author D. L. Oliver: Department of Neuroscience, University of Connecticut Health Center, Farmington, CT 06030-3401, USA. Email: doliver@neuron.uchc.edu

Abbreviations ABR, auditory brainstem response; BF, best frequency; CV, coefficient of variance; D-AP5, D(−)-2-amino-5-phosphonovaleric; eRs, effective series resistance; IC, inferior colliculus; ICC, central nucleus of the inferior colliculus; NBQX, 2,3-dioxo-6-nitro-1,2,3,4 tetrahydrobenzo[f]quinoxaline-7-sulfonamide; PSTH, post-stimulus time histogram; PTX, picrotoxin; seEPSC, sound-evoked excitatory postsynaptic current; seIPSC, sound-evoked inhibitory postsynaptic current.

Introduction

In the auditory system, the temporal code for sound is transmitted as action potentials from the cochlea to the cochlear nucleus, where the temporal pattern may be either preserved or altered (Rhode & Greenberg, 1992). Preservation is accomplished by specialised cellular mechanisms and glutamatergic synapses in some neurons that allow neuronal firing to phase lock precisely with their excitatory input (e.g. Borst & Sakmann, 1996; Gardner 1999; Borst & Soria van Hoeve, 2012; Golding & Oertel, 2012). Other neurons in the cochlear nucleus create new temporal patterns of neuronal firing (Young & Oertel, 2010). When auditory information reaches the inferior colliculus (IC), the primary integration centre of auditory pathways in the midbrain, the specialised excitatory synapses that mediate phase locking and temporal preservation are absent, and the temporal coding ability of a single neuron is less precise than in the relay synapses of the auditory brainstem. Nevertheless, IC neurons have diverse firing patterns in response to sound (Urban & Willott, 1979; Ehret & Moffat, 1985; Ehret, 1997; Rees *et al.* 1997; Brand *et al.* 2000), and these patterns may extract specific temporal features of sound (e.g. Rodriguez *et al.* 2010). However, the synaptic mechanisms that generate the diversity of temporal firing patterns in the IC are not known.

The integration of excitatory and inhibitory synaptic inputs over time is crucial for the coding of auditory information because sound changes rapidly over time (Wehr & Zador, 2003; Sun *et al.* 2010). The synaptic inputs to IC neurons are complex and arrive from ascending, local or descending sources. The IC has inputs from lower centres that may be either excitatory or inhibitory (e.g. Loftus *et al.* 2010). However, little is known about the temporal properties of these synaptic inputs in the IC, primarily because there are few direct measurements of the excitatory and inhibitory postsynaptic currents (EPSCs and IPSCs) evoked by sensory stimuli *in vivo* (Gittelman *et al.* 2012; Kuo & Wu, 2012; Li & Pollak, 2013; Xiong *et al.* 2013). Moreover, it is unclear how diverse firing patterns in the IC are generated by the interaction of excitatory and inhibitory synaptic inputs.

Here, we investigated whether excitatory and inhibitory synapses differ in their time course in response to sound *in vivo* and how they contribute to diverse firing patterns in the IC. To address these questions, we used *in vivo* voltage clamp recordings to isolate and investigate sound-evoked (se)EPSCs and seIPSCs in IC neurons in response to sustained tones; we also used modelling to assess the contribution of seEPSCs and seIPSCs to spike responses. We found that in most IC neurons, both excitatory and inhibitory synaptic currents are evoked by acoustic stimuli in the same ear. However, the seEPSCs and seIPSCs that were evoked by tones exhibited temporal patterns that varied in different ways. The seEPSC peak varied over a wide range from very early to much delayed (build-up), whereas the seIPSC peak was always early. Both seEPSCs and seIPSCs had a range of durations, but only the seIPSCs exhibited an off response. An integrate-and-fire computational model shows that the temporal pattern of spikes strongly reflected the time course of the seEPSCs, but the temporal pattern of spikes is modified by the properties of the seIPSCs. These results suggest that seEPSCs and seIPSCs have an asymmetric temporal interaction and that they contribute to diverse firing patterns in different ways. The excitatory inputs provide diverse patterns of membrane depolarization in different IC cells. In contrast, the inhibitory inputs are less temporally variable but may modify the neural response through small adjustments of latency, duration and amplitude.

Methods

Ethical approval

All experiments were approved by the Animal Care Committee at the University of Connecticut Health Center and were performed in accordance with institutional guidelines and the NIH *Guide for the Care and Use of Laboratory Animals*. All efforts were made to minimise the number of animals used.

Animals

Forty-three GAD67-GFP knock-in mice of either sex (Ono *et al.* 2005; Tamamaki *et al.* 2003) (postnatal day 26–42) were used in this study. Prior to 2006, knock-in mice were backcrossed against a Swiss–Webster background

(Acuna-Goycolea *et al.* 2005), and a colony of these mice was established in our facility. Breeding pairs consisted of one hemizygous and one wild-type littermate and were bred without backcrossing for >20 generations. The hemizygous offspring had a high expression of GFP in their brains, and the neonates (P0–2) were phenotyped by checking for fluorescence under blue light. We used both hemizygous littermates (Tg/+) and homozygous wild-type littermates (+/+).

Sound stimulation

Acoustic stimuli were generated by a TDT System 2 or 3 (TDT, Tucker Davis Technologies, Gainesville, FL, USA) under the control of customised MATLAB software (Brian Bishop, University of Connecticut Health Center; Marcel van der Heiden, University of Utrecht, Netherlands). All sounds were delivered by electrostatic speakers (TDT EC1) through small metal tubes (inner diameter, 1.10 mm). The sound system was calibrated from 60 to 50 000 Hz for System 2 and from 100 to 100 000 Hz for System 3. The calibration was performed at the end of the metal tubes with a ¼ inch microphone (Type 4135, Brüel & Kjaer, Naerum, Denmark). The stimuli were 200 ms pure tones or white noise with 5 ms rise and fall times. A stimulus duration of 100 ms was used in the pharmacological experiments (Fig. 1).

Surgical preparation

Animals were initially anaesthetised with a mixture of ketamine (100 mg kg^{-1}), xylazine (20 mg kg^{-1}) and acepromazine (10 mg kg^{-1}) and then maintained in an areflexive state with 0.5–1.0% isoflurane mixed with oxygen during the surgery and recordings. Vital signs were monitored with a non-invasive MouseOx Plus pulse oximeter (Starr Life Science Corp, Allison Park, PA, USA); body temperature was monitored with a rectal probe coupled to a digital thermometer and maintained at >35°C with a chemical isothermal heating pad (Grabber Inc., Grand Rapids, MI, USA). Surgery and recordings were conducted in a double-walled sound-attenuating chamber (IAC, Bronx, NY, USA).

A small craniotomy (1.5 mm × 1.5 mm) was performed over the right IC, and the dura was removed. After the craniotomy, the auditory brainstem response (ABR) to a click (0.5 ms) was routinely measured to verify that brainstem responses were normal ($n = 28$ animals). The ABR was measured with a Multiclamp 700B Amplifier, Digidata 1440A digitiser and Clampex 10.2 system (Molecular Devices, Silicon Valley, CA, USA) (filtered between 300 Hz and 3 kHz) with the TDT System 2 for 15 animals or with a TDT RA4PA four-channel preamplifier and TDT RA4LI headstage (1000× average, filtered between 500 Hz and 3 kHz) with the TDT System 3 for 13 animals. The threshold of the ABR was approximately 30 dB (left side 29.6 ± 0.57 dB, right side 28.9 ± 0.74 dB, $n = 28$, mean ± SEM). There was no difference in the threshold of ABRs between the genotypes or the stimulated sides ($P = 0.38$ and $P = 0.45$, respectively, two-way analysis of variance (ANOVA)). After the ABR recordings, the surface of the brain was covered with agarose gel (2% in 0.05 M phosphate buffer) to reduce brain pulsation.

Whole-cell recordings

Recording electrodes were made using borosilicate glass capillaries (34502–99, Kimble Chase, Vineland, NJ, USA) pulled on a Flaming/Brown P80/PC (Sutter Instruments, Novato, CA, USA) or PC-10 (Narishige, Tokyo, Japan) electrode puller. The electrodes were filled with a caesium gluconate-based internal solution (concentrations in mM: 125 caesium gluconate, 5 CsCl, 5 TEA-Cl, 10 Hepes-KOH, 1 EGTA, 4 MgATP, 0.3 Na_2GTP, 10 phosphocreatine, 1.5–6 QX-314, Neurobiotin 0.2%, pH 7.3), and their resistance was 3–5 MΩ. Whole-cell recordings were conducted using the standard blind technique (Margrie *et al.* 2002). The depth of the recording site ranged from 207 to 998 μm (415.1 ± 27.8 μm, $n = 40$). After a giga-seal configuration was obtained, the pipette capacitance was cancelled using a fast capacitance compensation circuit. The range of the pipette capacitance was 5–20 pF, which was within the range of fast capacitance compensation magnitude (0–36 pF). The cancellation was always checked visually by making the transient capacitance current almost invisible. After the whole-cell configuration was complete, the membrane capacitance was cancelled (147.0 ± 10.1 pF, $n = 40$). The membrane resistance was 455.8 ± 39.9 MΩ ($n = 40$). These values were higher than those used in previous studies of mice *in vivo* (Tan *et al.* 2007; Geis & Borst, 2013) due to the use of blockers in the internal solution. The series resistance (52.7 ± 2.7 MΩ, $n = 40$) was compensated for 60–70%. The liquid junction potential was estimated to be 10 mV and corrected (Sun *et al.* 2010). The data were filtered at 4 kHz and sampled at 10 kHz using a Multiclamp 700B Amplifier (Molecular Devices).

Separation of EPSC and IPSC

To separate the excitatory and inhibitory synaptic inputs, neurons were clamped at the assumed reversal potentials of the EPSC and the IPSC, and the responses to sound were recorded. Because EPSCs in the IC are suggested to be glutamatergic and IPSCs are GABAergic or glycinergic (Caspary *et al.* 1990), we assumed reversal potentials of EPSC (E_{epsc}) and IPSC (E_{ipsc}) of 0 mV (Ozawa *et al.* 1998) and −65 mV, respectively. To estimate E_{ipsc}, we used the Cl^- concentration of mouse blood (104–120 mM, Charles

River Laboratories). To verify that the assumed reversal potentials were appropriate, we performed experiments in which we added neurotransmitter receptor blockers to the agarose gel on the brain surface to administer the blockers continuously during the recordings (Fig. 1). To block the glutamatergic EPSCs, 2,3-dioxo-6-nitro-1,2,3,4 tetrahydrobenzo[f]quinoxaline-7-sulfonamide (NBQX) and D(−)-2-amino-5-phosphonovaleric (D-AP5) were applied (200 μM in agarose gel). To block the GABAergic or glycinergic IPSCs, picrotoxin (PTX) and strychnine were applied (200 and 100 μM in agarose gel, respectively). The recordings were performed at least 1 h after the start of the blocker application. The depth of the recording sites in this pharmacology experiment ranged from 226 to 502 μm (390.0 ± 41.4 μm, $n = 6$). The seIPSCs were recorded while blocking the EPSC with NBQX and D-AP5 (Fig. 1*A*), and the seEPSCs were recorded while blocking the IPSC by PTX and strychnine (Fig. 1*D*). The synaptic responses evoked by contralateral sound stimuli were recorded with different holding potentials that were changed in 20 mV steps above and below the assumed reversal potentials (Fig. 1). The reversal potential for the seIPSCs (Fig. 1*A*–*C*) was −65 mV, whereas the reversal potential for the seEPSCs (Fig. 1*D*–*F*) was 0 mV. For both the seEPSCs and the seIPSCs, the respective evoked currents were close to 0 pA (seIPSC peak amplitude: 3.3, 2.6 and −5.2 pA, $n = 3$; seEPSC peak amplitude: −13.6, −5.3 and 8.3 pA, $n = 3$; seIPSC charge transfer: 0.061, 0.074 and −0.40 pC, $n = 3$; seEPSC charge transfer: −0.65, 0.067 and 0.12 pC, $n = 3$), and the polarity of the currents was inverted (seIPSC, $n = 2$; seEPSC, $n = 3$).

The current–voltage plots of the seIPSCs showed rectification, i.e. that the outward current was larger than the inward current, and suggested that they may have different kinetics (Fig. 1*B* and *C*). This outward rectification may be due to the asymmetric Cl^- concentrations in the extracellular and intracellular spaces (Hodgkin & Katz, 1949; Barker & Harrison, 1988). To test this possibility, we compared the recorded data to a predicted current–voltage curve calculated using the GHK current equation (Fig. 1*B*, *C* right, grey lines). The GHK current equation is as follows:

$$I = \alpha V([Cl^-]_i - [Cl^-]_o e^{-zFV/RT})/(1 - e^{-zFV/RT})$$

where α is a constant; $[Cl^-]_i$ and $[Cl^-]_o$ are the internal and external concentrations, respectively, of Cl^- ions; and V is the membrane potential. In addition, z, F, R and T have their conventional meanings as follows: z, ion charge; F, Faraday's constant; R, gas constant; T, absolute temperature. The parameter α was varied using a least-squares algorithm. The values of the other parameters were as follows: $[Cl^-]_i = 10$ mM, $[Cl^-]_o = 115$ mM and $RT/zF = -26.6$.The curves for both the normalised peak amplitudes and charge transfers were well fitted to the GHK current equation (Fig. 1*B*, $\alpha = 0.00039$, $R^2 = 0.88$; Fig. 1*C*, $\alpha = 0.00041$, $R^2 = 0.93$), which supports the notion of asymmetric Cl^- concentrations. In terms of kinetics, GABAergic and glycinergic currents have been reported to be voltage dependent and to be accelerated by hyperpolarisation (Moroni *et al.* 2011). To determine whether this effect was present in our data, we measured the peak time and decay of the seIPSCs at different potentials. To evaluate the kinetics of isolated seIPSCs at different potentials, the decay time constant was measured by fitting the decay phase with a single exponential curve. Neither parameter showed a systematic voltage-dependent change (e.g. Fig. 1*A*, peak time 20.7, 20.9, 24.3, 20.4, 27.2 and 19.6 ms and decay time constant 20.8, 30.9, 101, 38.3, 38.3 and 12.2 ms at the holding potential of −5, −25, −45, −85, −105 and −125 mV, respectively).

The seEPSC exhibited a longer decay (Fig. 1*D*) and a larger charge transfer at depolarised potentials, resulting in an outward rectification (Fig. 1*F*) that was not obvious in the seEPSC's peak amplitudes (Fig. 1*E*). The outward rectification of the seEPSC was probably due to the unblocking of NMDA receptors at the more depolarised potentials. Most neurons in the IC are known to have NMDA receptors as well as AMPA receptors (Zhang & Kelly, 2001; Wu *et al.* 2004; Sivaramakrishnan & Oliver, 2006; Sanchez *et al.* 2007; Malmierca & Hackett, 2010). The NMDA channels require depolarising potentials to release the blockage of the channel by Mg^{2+} (Mayer *et al.* 1984).

These results showed that the reversal potentials of −65 and 0 mV were valid and that the neurons were voltage-clamped reasonably well in our *in vivo* whole-cell recordings even though the series resistances were higher (in pharmacological experiments, 45.5 ± 9.3 MΩ, $n = 6$, 60–70% compensated) than in conventional *in vitro* recordings. There was no significant difference in membrane resistance between the recordings with external blockers (428.5 ± 76.4 MΩ, $n = 6$) and without external blockers (460.9 ± 43.0 MΩ, $n = 34$, $P = 0.95$, Wilcoxon signed-rank test).

Recording procedure

Neurons were clamped at −65 mV to record the EPSCs. For 31 neurons, we presented tone bursts of 50–70 dB to determine the neurons' best frequency (BF). The BF was determined as the frequency that evoked the largest seEPSC. The recorded BFs were 2–22 kHz (mean ± SEM, 13.1 ± 0.84 kHz, $n = 31$). For one neuron out of 31, we used a broadband noise stimulus (bandwidth 10–50 kHz) in addition to the pure tone. In seven neurons, we only used noise, and we recorded only spontaneous currents in two neurons.

First, we determined the threshold as the lowest sound level that evoked a synaptic response. We presented a stimulus to the ear contralateral to the recording electrode and changed the sound intensity from 0 to 80 dB in 10 dB steps. The sound intensity was varied in a pseudorandom manner in all the experiments. In all cases, each tone was presented 10–20 times. The stimuli were repeated every 0.7 or 1.2 s. When repetitive stimuli evoked an obvious synaptic depression, the repetition rate was lowered to 2.2 s. After we recorded the responses at −65 mV, we changed the holding potential to 0 mV and repeated the same sound protocol.

Integrate-and-fire neuron model

We used an integrate-and-fire neuron model to evaluate the influence of the excitatory and inhibitory synaptic inputs on spike generation (Wehr & Zador, 2003; Sun *et al.* 2010):

$$C \times [V_m(t+\mathrm{d}t) - V_m(t)] = -\mathrm{d}t \times [G_e(t) \times (V_m(t)E_{epsc}) + G_i(t) \times (V_m(t)E_{ipsc}) + (V_m(t)E_r)/R_m]$$

where $V_m(t)$ is the membrane potential at time t, C is the whole-cell capacitance, G_e is excitatory conductance, G_i is inhibitory conductance, R_m is the resting leaky membrane resistance and E_r is the resting membrane potential. To evaluate the effects of R_m and E_r, R_m was varied from 80 to 600 MΩ and E_r was varied from −50 to −68 mV using the values for the IC reported in previous studies (Peruzzi *et al.* 2000; Sivaramakrishnan & Oliver, 2001; Ono *et al.* 2005; Tan *et al.* 2007; Geis & Borst, 2013). For whole-cell capacitance, we used a value close to the estimated values in previous current clamp recordings (50 pF) (Ono *et al.* 2005; Tan *et al.* 2007; Geis & Borst, 2013) instead of the value recorded by voltage clamp recordings in the present study. The whole-cell capacitance values estimated by voltage clamp were higher (see above; see also, Sivaramakrishnan & Oliver, 2001) than those estimated by current clamp (40–60 pF). We used the values in the current clamp recordings because the model is a simulation of a current clamp condition rather than a voltage clamp condition. The values in the voltage clamp recordings may reflect the space clamp range (Sivaramakrishnan & Oliver, 2001). The threshold of the spike was set at −48 mV. The rise, decay and refractory times of the spike were set at 1, 1 and 5 ms, respectively. The peak and after-hyperpolarising potentials were set at 20 and −80 mV, respectively.

Using the model, we evaluated how the peak time and the width of the seIPSCs contribute to spike generation. To evaluate the effect, we generated the spike histogram while introducing jitter into the values for V_m, G_e and G_i. To add jitter to the V_m, white noise was added to the right side of the equation. The magnitude of the noise was adjusted to make the SD of V_m equal 1.25 mV. The sizes of G_e and G_i were jittered by multiplying randomised scaling factors of 1 ± 0.182 and 1 ± 0.188, respectively. The coefficient of variation (SD/mean, CV) of the recorded responses was measured (seEPSCs, 0.182 ± 0.017, $n = 28$; seIPSCs, 0.188 ± 0.026, $n = 20$) and assigned as the limits of scaling factors. The CVs were measured in the maximum evoked responses. R_m and E_r were set to 140 MΩ and −56 mV, respectively. The responses of the model were repeated 100 times to compose the histograms. To generate G_e and G_i, we used the α-function or a modified α-function:

$$\text{Modified } \alpha\text{-function} = K \times (1 - e^{-t/t_1})^s \times e - t/t_2$$

where s is a temporal scaling factor. G_e and G_i were designed to simulate the evoked responses to 200 ms tone stimuli. The rise of the conductance was set to start 12 ms after the assumed sound onset. After the 200 ms from the assumed sound onset, the conductances were set to decay exponentially with a time constant of τ_3. We used three G_e models with different time courses. For G_i, we systematically changed the peak times and the durations to study their effects on spike generation. To create G_i with different durations, keeping the rise phase constant, we combined the rise phase of the standard G_i curve (peak time, 42.0 ms; 25% width, 140.1 ms) with the decay phase of the G_i curves of different durations (Table 3).

Synaptic current analysis

Most analyses were performed using Clampfit 10.2 software (Molecular Devices), MATLAB, R (version 3.0.1, The R Foundation for Statistical Computing, Vienna, Austria) and Origin 7.5 (OriginLab, Northampton, MA, USA). Spontaneous EPSCs and IPSCs were collected from 5–10 s recordings. The spontaneous inputs were detected using the template search program of Clampfit 10.2. To measure their kinetics, we averaged at least 20 detected spontaneous inputs. We measured the 10–90% rise time and decay time constants of the averaged spontaneous inputs. The decay time constant was measured by fitting the decay phase of the averaged spontaneous input with a single exponential curve. We averaged at least eight seEPSCs and seIPSCs. To evaluate the size of the synaptic inputs, we used two parameters: the peak amplitude and the charge transfer of the currents. The peak amplitude was measured from the baseline. The peak was detected as the point with the maximum change from baseline in the recorded time (0.5, 1 or 2 s). The charge transfer was measured as the evoked currents integrated through time. Both parameters were measured from the averaged current. To evaluate the duration of the evoked currents, we measured the width between the 25% rise and decay

points of the currents (25% width). We used the 25% width, instead of the conventional half width, because the 25% width reflects the difference in the persistent component of the evoked currents better than the half width.

The effective series resistance (eR_s) was calculated as follows:

$$eR_s = \text{series resistance} \times (100 - \%\ \text{compensation})/100.$$

The errors of the holding potentials due to the uncompensated series resistance were estimated by the following equation:

$$\text{Error} = \text{holding } current \times eR_s.$$

We excluded the data with an error greater than 10 mV. The average value of the error was 1.44 ± 0.19 mV ($n = 35$) for EPSCs and 1.93 ± 0.33 mV ($n = 27$) for IPSCs. Small error values were likely because of the high membrane resistance due to the use of internal blockers.

Validation of the model

To validate the model, we compared the responses of the model with the extracellularly recorded spike responses in three neurons. In these neurons, we recorded both synaptic responses and spike responses. The spike responses were recorded before a break-in for whole-cell recordings. The seEPSCs and seIPSCs were each recorded ten times. These synaptic inputs were converted into conductances. The modelled spike responses were calculated using all combinations of the EPSC and IPSC. In these models, we did not apply jitter to the membrane potential. The seEPSCs and the seIPSCs were converted into conductance to facilitate visual comparison. To convert them into conductances, the seEPSCs and the seIPSCs were subtracted from the baseline and divided by the driving force (65 mV).

The extracellular spikes were recorded in the voltage clamp mode instead of the conventional current clamp mode to improve the stability during the transition from giga-seal extracellular to whole-cell intracellular recordings. To determine whether there was a difference between the two recording modes in the observation of firing patterns, we conducted giga-seal, cell-attached recordings in four additional test neurons and compared the evoked spike responses recorded in the voltage clamp mode to those recorded in the current clamp mode (data not shown). In all four recorded neurons, there was no significant difference in post-stimulus time histogram (PSTH) distribution between the two recording modes ($P = 0.96$, 0.49, 0.61 and 0.25, Kolmogorov–Smirnov test; $P = 0.99$, 0.67, 0.48 and 0.19, Wilcoxon signed-rank test).

Statistical analysis

The data were first subjected to the Shapiro–Wilk normality test. When the data had a normal distribution, they were subjected to statistical evaluation using the two-tailed F test, two-tailed Student's t test or an analysis of variance (ANOVA) with a *post hoc* comparison. Otherwise, they were evaluated by Mood's dispersion test, the Wilcoxon signed-rank test and/or the Kolmogorov–Smirnov test. For certain data, we calculated the correlation coefficient (R), which was also statistically tested by two-tailed Student's t test (Zar, 1998). The criterion for significance was defined as $P < 0.05$. When two parameters had a significant correlation coefficient (R), we performed a regression test and plotted a regression line. Values are expressed as mean ± SEM unless otherwise indicated.

Chemicals

Neurobiotin was obtained from Vector Laboratories (Burlingame, CA, USA). All other chemicals were from Sigma Aldrich (St Louis, MO, USA).

Space clamp problem

With a voltage clamp at the neuronal somata, current inputs on the dendrite may be slowed, attenuated and dependent on the dendritic distance (Williams & Mitchell, 2008). The dendritic electrical properties of the IC neurons are not established; however, a distance-dependent attenuation of dendritic synaptic input may occur. Thus, our recordings may be dominated by the proximal synapses. We believe these proximal synapses were well clamped, as our reversal potentials were close to the theoretical values (Fig. 1) despite possible filtering by dendritic cable properties. After the recording, the animal was fixed and histology was performed to investigate the morphology with Neurobiotin labelling. All neurons recovered in this study ($n = 10/38$) showed dendritic filling (data not shown). This observation supports the notion that the internal solution with blockers diffused into the dendrites and reduced any space clamp error.

Data from transgenic and wild-type mice

We investigated whether there was any difference in the sound evoked PSCs between the transgenic GAD67 knock-in and wild-type mice (data not shown). There was no significant difference between the wild-type (14 seEPSCs, 7 seIPSCs) and transgenic animals (9 seEPSCs, 6 seIPSCs) for the parameters of the time course and the size of evoked PSCs. Because there was no difference in the auditory brainstem response thresholds (see Methods) or

in the synaptic currents, we did not separate the recordings from the knock-in and wild-type littermates.

Estimation of the series resistance error of evoked responses

To estimate the effect of the series resistance on sound evoked synaptic responses, we synthesized the evoked responses, convolving the assumed unitary responses with presynaptic PSTHs with different time courses (see Fig. 11). The unitary responses were modelled using α-functions.

$$\alpha\text{-function} = K \times (1 - e^{-t/\tau_1}) \times e^{-t/\tau_2}$$

where K is a scaling constant, and τ_1 and τ_2 are time constants. To model unitary responses with different eRs, K, τ_1 and τ_2 were set as follows: 22.3 pA, 1.5 ms and 5.3 ms for 5 MΩ eRs, 15.6 pA, 1.9 ms and 7.5 ms for 15 MΩ eRs, and 9.2 pA, 2.5 ms and 10.4 ms for 25 MΩ eRs, respectively. To model presynaptic PSTHs, we also used α-functions. We used 13 combinations of τ_1 and τ_2 to cover the different temporal patterns. The combinations are: $\tau_1 = 1$ ms and $\tau_2 = 10, 50, 100, 500$ ms; $\tau_1 = 10$ ms and $\tau_2 = 10, 50, 100, 500$ ms; $\tau_1 = 50$ ms and $\tau_2 = 500$ ms; and $\tau_1 = 100$ ms and $\tau_2 = 10, 50, 100, 500$ ms. K was adjusted to make the maximum value 20, and a latency of 12 ms was used. The generated curve was divided into 5 ms bins and converted into a PSTH. When convolving the PSTH with unitary responses, spikes were assigned to each bin following the PSTH, and in each bin the spikes were distributed randomly. The convoluted responses were synthesized 25 times and averaged. The temporal parameters were measured using Clampfit 10.2.

Results

We investigated whether the temporal properties of excitatory and inhibitory synaptic responses to sound differ in neurons of the central nucleus of the IC (ICC) in mice *in vivo*. To measure the excitatory and inhibitory synaptic currents independently, we recorded sound-evoked responses at two different holding potentials (−65 and 0 mV) determined empirically to be the reversal potentials of the IPSC and the EPSC, respectively (see Methods). The present results are based on the synaptic responses evoked by sound in 38 neurons (including six neurons described in the Methods). We studied the temporal properties of the synaptic currents in response to 200 ms pure-tone stimuli at the BF of the

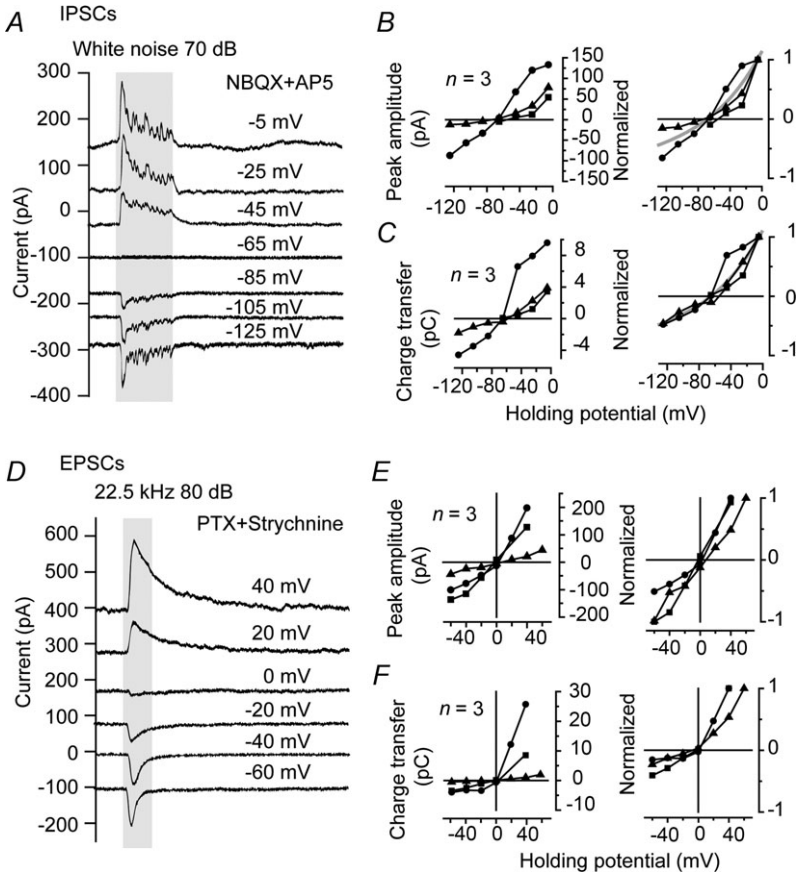

Figure 1. When measured *in vivo*, the EPSCs' reversal potential was 0 mV and the IPSCs' reversal potential was −65 mV
A, averaged selPSCs isolated by blocking excitatory synaptic inputs with NBQX and D-AP5. Ten repetitions of 200 ms white noise (10–50 kHz, 70 dB) were delivered to the contralateral ear. The holding potentials are shown with each trace. *B* and *C*, *I–V* plots of the selPSCs ($n = 3$). *D*, averaged seEPSCs isolated by blocking the inhibitory synaptic inputs with PTX and strychnine. *E* and *F*, *I–V* plots of the seEPSCs ($n = 3$). *B* and *E*, peak amplitude. *C* and *F*, charge transfer. The left plots are original *I–V* plots, and the right plots are normalised *I–V* plots. The grey curves in the normalised plots (*B*, *C*) are the predicted curves from the Goldman–Hodgkin–Katz current equation.

neuron and delivered to the contralateral ear. This data set includes the evoked seEPSCs from 30 neurons and the evoked seIPSCs from 21 neurons. Two neurons were excluded. In one, we failed to record enough seEPSCs (>8) for averaging. In another, the neuron responded only to the tone offset rather than the current onset (29.3 ms after the tone offset).

Most recordings were localised to the ICC based on the recording depth and latency. Thirty of 40 neurons were 250–550 μm below the surface, corresponding to the dorsal and central parts of the mouse ICC, and six neurons were 600–1000 μm below the surface. Thus, 90% of the recordings were at a depth below 250 μm. Our recorded current onsets were consistent with ICC recordings, as 74 and 75% of seEPSCs and seIPSCs, respectively, had a current onset shorter than 20 ms (seEPSC, median 14.9 ms, $n = 27$; seIPSC, median 14.1 ms, $n = 20$).

This study addresses the general question of how the seEPSC and seIPSC generate the firing pattern of the neuron. To do so, we first show how seEPSCs and seIPSCs differ in their temporal patterns. This includes the synaptic currents during and after the offset of sound. The next part details the relationships of the seEPSC and seIPSC recorded in the same neuron in response to the same acoustic stimulus. Finally, we use the temporal patterns of the recorded seEPSCs and seIPSCs to model and evaluate their respective contributions to the firing pattern of the neuron.

seEPSCs had more diversity in peak times than seIPSCs

The time course of the seEPSCs varied in ways that the seIPSCs did not. In Fig. 2*A*–*F*, we show the seEPSCs and seIPSCs to tones from five neurons (*D* and *E* are the same neuron). Two distinct types of seEPSCs were observed: early-peaked (Fig. 2*A*–*C*) and build-up seEPSCs (Fig. 2*D*). The early-peaked seEPSCs varied from a transient (Fig. 2*A*) to a more sustained current (Fig. 2*B* and *C*). Early-peaked transient seEPSCs had a rapid onset and a rapid decay with a peak time of <100 ms and a duration of <50 ms (Fig. 2*G*, *H*). The duration was calculated as the width of the current at 25% amplitude (Fig. 2*H*). Early-peaked sustained seEPSCs had a rapid onset and a slower decay; this was an adapting response with a duration >50 ms. The second type of seEPSCs (Fig. 2*D*) had a slowly rising onset phase that peaked more than 100 ms after the tone onset (the build-up; the median of current onset was 13.6 ms, $n = 6$). In contrast, the seIPSCs exhibited only early-peaking responses (Fig. 2*E*, *F*).

The population data showed clearly that the peak times of the seEPSCs were distributed more broadly than those of the seIPSCs (Fig. 2*G*). We compared the mean peak times of seEPSCs and seIPSCs across all intensity levels (histograms, Fig. 2*G*; mean seEPSC peak time, 62.5 ± 62.5 ms, $n = 28$; seIPSC peak time, 41.2 ± 13.9 ms, $n = 20$) and found a significant difference between the seEPSCs and the seIPSCs in dispersion ($P < 0.001$, Mood's dispersion test) but not in the median ($P = 0.70$, Wilcoxon signed-rank test). In contrast to the peak times, the durations of the seEPSCs and seIPSCs covered a similarly broad range (Fig. 2*H*). The seEPSC mean 25% width was 117.4 ± 90.4 ms; the seIPSCs width was 141.5 ± 76.3 ms. There was no significant difference between the seEPSCs and the seIPSCs in either the dispersion or the median ($P = 0.11$, Mood's dispersion test; $P = 0.19$, Wilcoxon signed-rank test).

The seEPSC peak times varied little with increasing sound levels. To evaluate the invariance of peak times against sound levels, we measured the CV of the peak times across different sound levels. We recognized that the peak time was 'shifted' when CVs were higher than 0.2. The neurons with high thresholds (≥70 dB, $n = 5$) were excluded from this analysis. Most neurons showed invariant peak times across different sound levels (Fig. 2*G*, upper panel) and had CVs lower than 0.2 (78%, 18/23). These 18 neurons contained 15 early-peaked seEPSCs and three build-up seEPSCs. Among five neurons with CVs higher than 0.2, two remained as early-peaked responses (minimum peak time, 21.7 and 23.1 ms, maximum peak time, 59.6 and 37.0 ms, CV, 0.51 and 0.21, respectively). The seEPSCs changed from early-peaking to build-up in two neurons (peak shift, 147.7 and 96 ms, CV, 0.59 and 0.37, respectively); in one neuron, the seEPSCs changed from build-up to early-peaking (peak shift, 86.9 ms, CV, 0.55). For most seIPSCs, the peak time was also invariant with sound levels (Fig. 2*G*, lower panel). Excluding the neurons with high thresholds (≥70 dB, $n = 7$), 85% of neurons (11/13) had CVs lower than 0.2. Two neurons had CVs of 0.24 and 0.23, and peak time shifts of 20.7 and 33.9 ms, respectively. The level invariance of peak times in seIPSCs and most seEPSCs suggests that this temporal property is a fixed property of the synapse and not merely due to a stronger input at higher sound levels.

In contrast to peak times, there was a tendency for the PSC to increase in duration when the sound level increased (Fig. 2*H*). This tendency was more prominent in seIPSCs. In the same manner as the peak time, we measured the CVs of 25% width and evaluated the shifts in duration when the sound level increased. Sixty-one percent of IPSCs (8/13) had CVs higher than 0.2, and showed a level-dependent increase in duration, while 43% of seEPSCs (10/23) had CVs higher than 0.2 and an increase in duration. No sound evoked PSCs showed a significant level-dependent decrease in duration.

We observed a positive correlation between the seEPSCs peak time and the 25% width (Fig. 2*I*; seEPSC red, $R = 0.70$, $P < 0.001$; seIPSC blue, $R = 0.33$, $P = 0.15$). The early-peaking seEPSCs (Fig. 2*I*, right panel) had a continuous distribution with a gradual change from

early-peaking transient seEPSCs (Fig. 2*A*) to early-peaking sustained seEPSCs with longer latency peak times and durations (Fig. 2*B*, *C*). The seIPSCs also showed a continuous distribution in their peak times and durations (Fig. 2*H*). Interestingly, the highly transient responses were not seen in seIPSCs. No seIPSC duration was shorter than 36 ms (Fig. 2*I*, right panel), while some seEPSC durations were shorter than 36 ms ($n = 6$).

Offset responses were unique to seIPSCs

In addition to different temporal patterns during sound presentation, the seEPSCs and the seIPSCs were distinguished by their offset responses. Close to one-third of the neurons had an seIPSC at the offset of the tone, but an offset response was not observed in the seEPSCs. To evaluate the off responses quantitatively, we measured the off-peak charge by calculating the charge of the offset

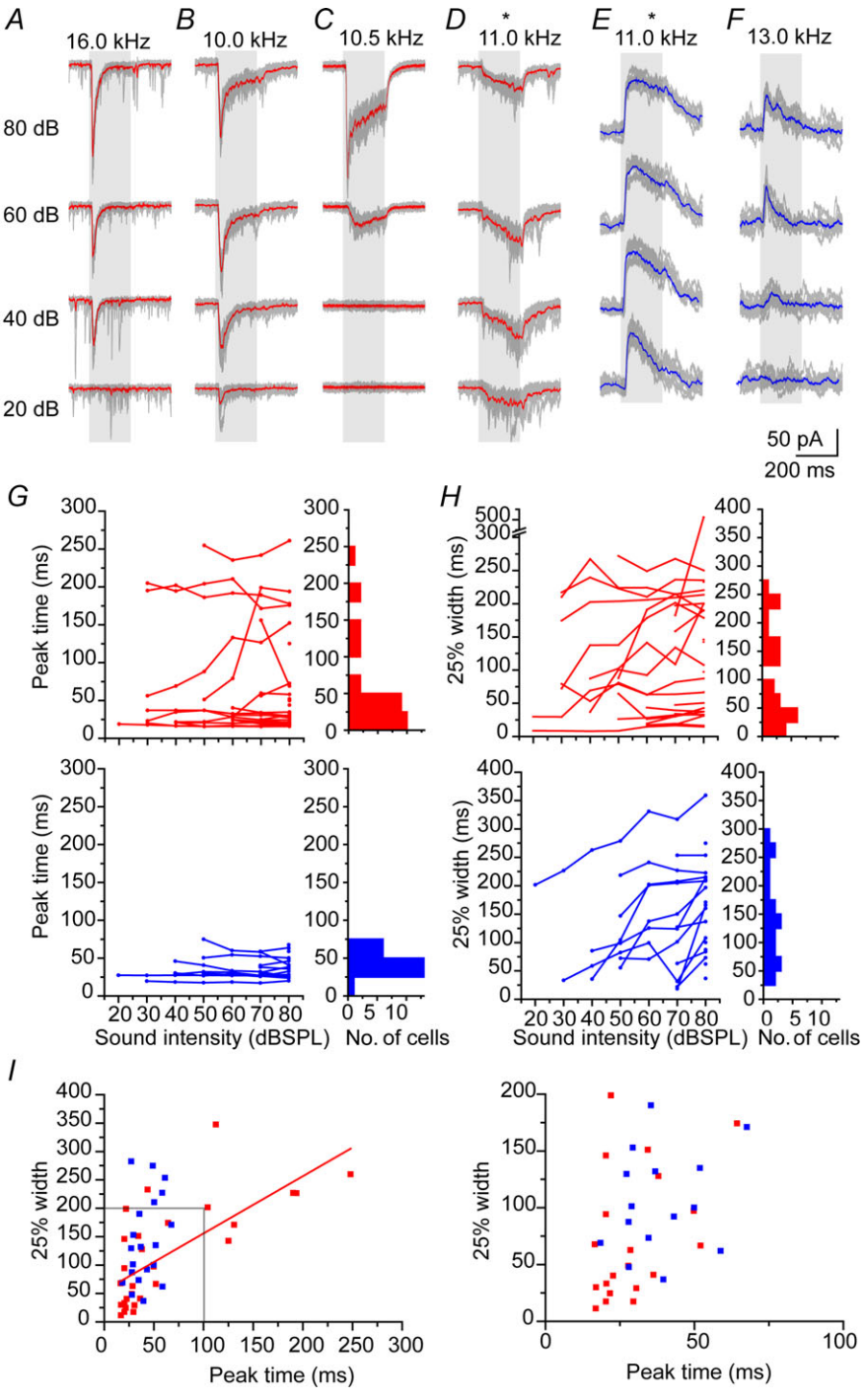

Figure 2. The seEPSCs and seIPSCs differ in peak latency and duration; seEPSCs showed more variability and the shortest latencies and durations
A–F, responses to BF tones at four sound intensity levels are shown for five neurons (∗*D* and *E* are the same neuron). Grey traces are 10 superimposed responses to contralateral BF tones. The red (*A–D*, seEPSCs) and blue (*E*, *F*, seIPSCs) traces are the averaged traces. Grey bars indicate the 200 ms tone presentation. *A–C*, early-peaking seEPSCs. *D*, build-up seEPSC. *E* and *F*, seIPSCs of longer and shorter duration. *G* and *H*, the peak time (*G*) and 25% width to measure of duration (*H*) plotted against sound intensity. Upper panel, seEPSC (red). Lower panel, seIPSC (blue). For each neuron, we calculated the mean peak times and 25% widths of the responses to different sound intensities. The mean values are plotted in histograms (right panels). *I*, the peak time is plotted against the 25% width. The right panel shows the magnified plot of the grey box in the left panel.

peak to a point 10 ms later using the current level at sound termination as a baseline (Fig. 3*A*). In response to 80 dB tones, seven neurons showed an offset response (offset$^+$) with a positive charge greater than 20 fC (72.2 ± 21.3 fC, $n = 7$, Fig. 3*B*). In contrast, the neurons with no offset charge (offset$^-$) had either negative off-peak charge values (−43.0 ± 18.7 fC, $n = 11$) or a value near zero (0.76, $n = 1$). The seIPSCs with a large off-peak charge (Fig. 3*C*, right panel) usually had a distinct hump after the sound offset, unlike the seIPSCs that decayed monotonically (Fig. 3*C*, left panel). For seIPSCs evoked by 80 dB tones, the offset response peaked at 19.8 ± 3.2 ms after the stimulus offset ($n = 7$). The presence or absence of an offset response was consistent over a range of supra-threshold sound levels (Fig. 3*D*, measured from 10 dB above the onset threshold). In some neurons with an offset$^+$ response, the off-peak charge values changed from negative to positive with increasing sound intensity (Fig. 3*D*). This suggests that the thresholds of the offset responses were higher than the onset responses. Offset$^+$ neurons could not be distinguished from offset$^-$ by the BF (offset$^+$, 13.9 ± 1.3 kHz, $n = 7$; offset$^-$, 12.1 ± 1.2 kHz, $n = 12$, $P = 0.30$, Student's t test). There was also no significant difference in the temporal properties of the seEPSCs or the seIPSCs for the offset$^+$ and offset$^-$ neurons (Fig. 3*E–H*, seIPSC peak time: offset$^+$, 40.0 ± 5.6 ms; offset$^-$, 40.4 ± 3.9 ms; seEPSC peak time: offset$^+$, 70.7 ± 25.8 ms; offset$^-$, 67.4 ± 22.3 ms; seIPSC 25% width: offset$^+$, 158.1 ± 35.8 ms; offset$^-$, 138.4 ± 19.2 ms; seEPSC 25% width: offset$^+$, 96.7 ± 33.9 ms; offset$^-$, 152.7 ± 30.4 ms; $P = 0.49$, 0.24, 0.71, 0.84, respectively, Wilcoxon signed-rank test). These data suggest that the source of the offset may be independent of the sources of the IPSCs during the sound stimulation.

Sequences of seEPSCs and seIPSCs within the same neuron

The pooled population data above revealed that seEPSCs and seIPSCs had different time courses. To examine how seEPSCs and seIPSCs interact in an individual neuron,

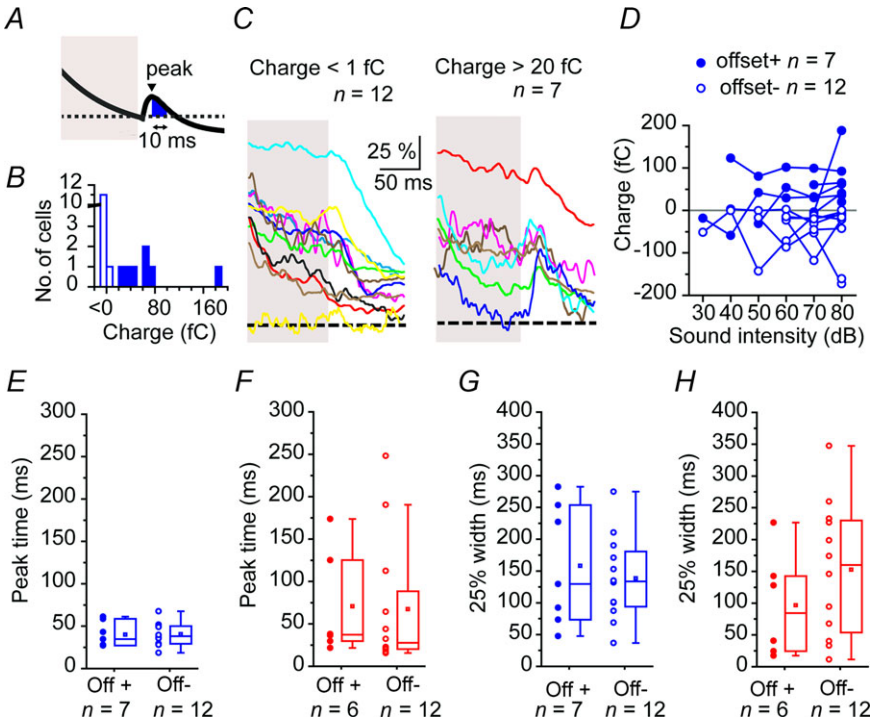

Figure 3. Some seIPSCs respond to the offset of sound
A, an illustration of the method to evaluate offset responses. The dotted line indicates the current level at the sound termination. The filled blue region indicates the off-peak charge. *B*, bar chart of the off-peak charges in response to 80 dB BF tones. Blank bars indicate cells with small values. The bin size was 10 ms. *C*, traces of the neurons with off-peak charge <20 fC (left panel) or >20 fC (right panel). The currents are normalised and low pass filtered (300 Hz). Only the current traces 100 ms before and after the sound termination are presented. The grey box indicates the sound presentation. *D*, the plots of off-peak charge at different sound intensities. *E–H*, comparison of temporal parameters in seIPSC off+ and off– neurons. Box plots are presented with raw data points. Boxes represent the 25th and 75th percentiles within which the small filled square and the line represent the mean and median, respectively. The whiskers represent the 10th and 90th percentiles. Blue, seIPSC; red, seEPSC. *E*, peak time of seIPSCs. *F*, peak time of seEPSCs. *G*, 25% width of seEPSCs. *H*, 25% width of seIPSCs.

we compared the temporal parameters of the paired seEPSCs and seIPSCs within the same cell. In 19 neurons, we successfully recorded both excitatory and inhibitory responses to the same BF tones. For this comparison, we used the responses at the sound intensity at which the seEPSCs were the largest (80 dB in 18 neurons, 30 dB in one neuron).

The temporal parameters of seEPSCs and seIPSCs within the same neuron displayed several patterns. For the population as a whole, there was a poor correlation between the peak times of the seEPSCs and the seIPSCs in the same neuron (Fig. 4*A*, upper left panel; $R = -0.11$, $P = 0.64$). However, when an seEPSC had a peak time less than 60 ms, it preceded the seIPSC in most neurons (12/13) (Fig. 4*A*, upper right panel; ratio: 1.78 ± 0.18, $n = 12$). In contrast, when an seEPSC peak time was greater than 60 ms, it followed the seIPSC (Fig. 4*A*, upper right panel; ratio: 0.32 ± 0.09, $n = 6$). These temporal sequences of the peak times of seEPSCs and seIPSCs are related to the distributions of the peak times of seEPSCs and seIPSCs (Fig. 4*A*, lower panel). Similar to the pooled data (Fig. 2*G*), the peak times of the seEPSCs were distributed more broadly than seIPSCs (Fig. 4*A*, lower panel); seEPSCs had the short and long peak times that seIPSCs did not have.

A similar comparison of the duration of paired currents showed a similar pattern for the seIPSCs paired with shorter or longer seEPSCs (Fig. 4*B*, upper right panel). Although the correlation of seEPSC and seIPSC duration was weak (Fig. 4*B*, upper left panel, $R = 0.48$, $P = 0.038$, when one outlier was excluded, $R = 0.36$, $P = 0.12$), the seEPSC with a duration shorter than 100 ms preceded a longer seIPSC in most neurons (8/9) (Fig. 4*B*, upper right panel; ratio: 3.86 ± 0.71, $n = 8$). When the duration of the seEPSC was longer than 100 ms, the seIPSC could be either shorter (4/10) or longer (6/10) (ratio: 0.99 ± 0.17, $n = 10$). These results show that the seIPSC was consistently longer in duration when the seEPSC was transient, but the duration of the seIPSC was less predictable when the seEPSC was more sustained.

In contrast to the temporal parameters, the sizes of seEPSCs and seIPSCs within the same neurons a positive correlation. Both the amplitude and the charge transfer of the seEPSCs and the seIPSCs within the same neuron (Fig. 5*A* and *B*, left panels) were positively correlated (peak amplitude, $R = 0.74$, $P < 0.001$; charge transfer, $R = 0.64$, $P = 0.003$). Although they were correlated, the ratios of IPSC to EPSC varied from cell to cell (Fig. 5*A* and *B*, right panels). Most neurons (63%; 12/19) had larger seIPSCs as measured by the peak amplitude (Fig. 5*A*, right panel; ratio: 1.36 ± 0.25, $n = 19$). More neurons (15/19) also had larger seIPSCs when the charge transfer was measured (Fig. 5*B*, right panel; ratio: 2.57 ± 0.86, $n = 19$). The tendency for seIPSCs to be larger may reflect the longer duration of seIPSCs in our sample (Fig. 4*B*).

The effects of seIPSC temporal properties on firing pattern

Our recordings of synaptic currents revealed that seEPSCs and seIPSCs had different time courses and formed an asymmetric pattern of interaction. How do these currents interact to create the firing patterns in the post-synaptic IC neurons? To answer the question, we used an integrate-and-fire model to generate the spike responses to given synaptic inputs. The predicted spike rates and latencies are shown in Fig. 6 as they result from the interaction of the excitatory conductance (G_e), inhibitory conductance (G_i), membrane resistance (R_m) and resting membrane potential (E_r) over the ranges observed in our recordings and in previous studies. In the following sections, using the model, we show how the temporal patterns of seIPSCs influence the firing pattern.

Effect of seIPSC peak time. How does the peak time of seIPSCs influence the firing pattern of the IC neuron? We simulated the temporal patterns for transient (G_e1), early-peaking-sustained (G_e2) or build-up (G_e3) seEPSC types (Table 1). To investigate the effect of seIPSC peak time on the firing pattern (Fig. 7), we used G_i peak times that ranged from 26.7 to 69.7 ms, the same range seen in our recorded G_i peaks (Fig. 2*G*, *I*). The 25% width of G_i was set to 142 ms (Table 2), and G_i was set at 1, 2 or 3 nS. G_e was constant at 2 nS. To generate PSTHs, jitter was added to G_e, G_i and the membrane potential set to -56 mV. In general, the modelled PSTH responses showed different firing patterns corresponding to the different excitatory inputs and reflected their time course (Fig. 7*A*–*C*).

When the excitatory conductance was transient (Fig. 7*A*, *D*), the change of the seIPSC peak had a large impact on spike firing rate when the G_i was large and was close to the G_e peak. The firing probability decreased, and the effect increased as the size of G_i increased (Fig. 7*D*, upper). Spike latency was unaffected (Fig. 7*D*, lower).

When the excitatory conductance was an early-peaking sustained G_e, the shape of the PSTH changed from sustained to transient with changing G_i peak. The onset of spiking was suppressed when the G_i and G_e peaks were close (Fig. 7*B*). As the G_i peak increased in latency and moved away from the G_e peak, the onset portion of the response increased in firing probability, but the sustained portion of the response was suppressed. This change in pattern was not reflected in the number of spikes per trial (Fig. 7*E*, upper) as the changes in the onset and sustained portions of the response counterbalanced each other. In addition to the peak time changes, the overall firing rate was strongly reduced as the G_i grew larger (Fig. 7*E*, upper). Spike latency also decreased with large G_i (Fig. 7*E*, lower).

When the excitatory conductance was a build-up G_e (Fig. 7*C*, *F*), the rising phase of the PSTH was slower and the overall PSTH did not show a substantial change

in shape with increasing G_i peak time. When G_i was greater than 2 nS, the firing rate decreased slightly with an increasing G_i peak time (Fig. 7*F*, upper), and the spike latency showed a modest increase (Fig. 7*F*). In summary, these results show that the excitatory inputs are critical to shape the general firing pattern, but the amplitude and rise phase of the inhibitory conductance can influence the rate and/or the time course of firing.

Effect of seIPSC duration. To investigate the effect of the G_i duration on the firing pattern (Fig. 8), the peak time of G_i was kept constant (Table 3), but the G_i duration was varied. To do so, the 25% width of G_i was varied from 39.2 to 281.5 ms (Fig. 8*A*–*F*) to match the range of the 25% widths in our recorded seIPSCs (Fig. 2*H*).

Again, the early-onset sustained firing pattern was altered more than the transient or build-up patterns by changing the duration of G_i. The onset components of the transient (Fig. 8*A*) and early-peaking sustained G_e were unaffected (Fig. 8*B*). However, the sustained firing to the latter was suppressed as the G_i duration increased (Fig. 8*B*). Thus, the firing rate decreased with an increased G_i duration for the early-peaked sustained G_e (Fig. 8*E*) but less so for the transient and build-up G_e (Fig. 8*D*, *F*). The spike latency was unaffected by the increases in G_i duration and amplitude for the transient pattern, increased to a small extent for the sustained pattern when G_i was 3 nS, and increased for the build-up G_e as the G_i duration grew longer and increased in amplitude (Fig. 8*C*, *F*). In summary, the changing durations of inhibitory inputs profoundly modify the early-peaked sustained firing pattern.

To validate our model, we compared PSTHs from recordings to results of the model in the same neuron. We recorded spikes in response to white noise in cell-attached mode and then completed a whole-cell configuration to record the seEPSCs and seIPSCs. Figure 9 shows the results from three neurons. The model predicted the

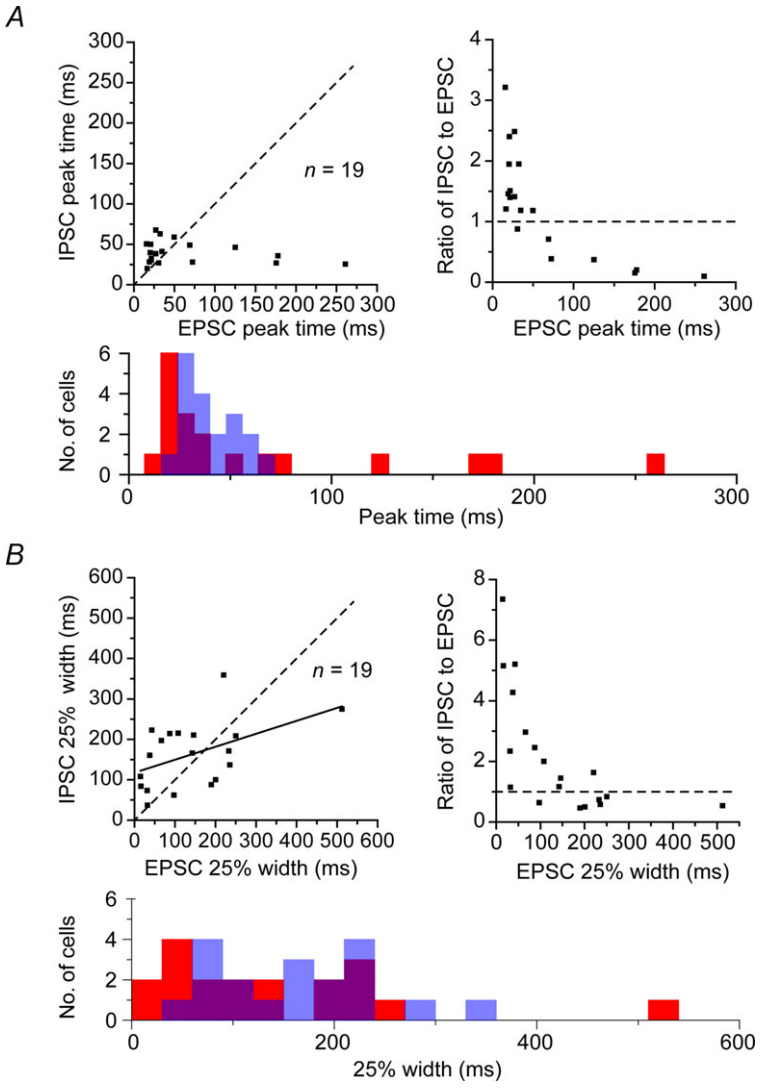

Figure 4. The temporal parameters of seEPSCs and seIPSCs recorded from the same neuron were poorly correlated; however, the fastest EPSCs always preceded the IPSCs, and the IPSCs always preceded the slowest EPSCs
The peak time (*A*) and 25% width (*B*) for seEPSCs and seIPSCs recorded from the same neuron. The upper left panels show the seEPSCs plotted against the seIPSCs. Dotted lines are lines of unity. The upper right panels show the seIPSC/seEPSC ratio plotted against the seEPSCs. Dotted lines indicate the level of 1. In *B*, the black line indicates a linear fit ($y = 117.61 + 0.32x$). The lower panels are histograms of the distributions of seEPSCs (red) and seIPSCs (blue).

spike responses accurately for neurons with a transient or build-up EPSC when appropriate R_m and E_r values were chosen. There were no significant differences between the firing pattern predicted by the model using the recorded seEPSC and seIPSC and the actual spikes obtained from the same cell in the cell attached mode ($P = 0.33$ and 0.18, respectively, Kolmogorov–Smirnov test, Fig. 9).

The series resistance effect did not change the overall shapes of sound-evoked synaptic currents

Although unlikely, it is possible that the variability in the seEPSC time course was an artefact due to a high effective series resistance (Williams & Mitchell, 2008) (eRs, see Methods), i.e. the uncompensated series resistance. There was no correlation between the size of eRs and the temporal pattern (Fig. 10*A*, *B*; seEPSC: $R = -0.26$, -0.081, $P = 0.19$, 0.68 for peak time and 25% width, respectively; seIPSC: $R = -0.079$, 0.0045, $P = 0.74$, 0.99). Peak amplitude and charge transfer were also uncorrelated with eRs (Fig. 10*C*, *D*; seEPSC: $R = 0.043$, -0.109, $P = 0.82$, 0.58 for peak amplitude and charge transfer, respectively; seIPSC: $R = 0.013$, 0.071, $P = 0.96$, 0.77). We did find a negative correlation between the peak amplitude of the spontaneous EPSC and series resistance (Fig. 11*F*). However, a model of this effect on the sound-evoked current showed that although there was an effect of slowing and reducing the current, it could not account for the variations in the temporal patterns of the seEPSCs (Fig. 11*I*–*M*).

Discussion

In the present study, we examined the temporal properties of the excitatory and inhibitory inputs in the auditory midbrain. We found that the time courses of seEPSCs and seIPSCs are asymmetric in response to the same fixed amplitude of 200 ms tones. The peak times of seEPSCs varied over a wider range than the seIPSCs. When recorded from the same neuron, the early-peaked transient seEPSC peaks usually preceded seIPSC peaks, while those of the late-peaking seEPSCs followed seIPSC peaks. The temporal parameters of seEPSCs and seIPSCs in the same neuron were poorly correlated, while the size parameters of them were positively correlated. Using an integrate-and-fire model based on our recordings, we showed how the temporal properties of the synaptic currents may produce different firing patterns. Our observations suggest that there are distinct contributions of excitatory and inhibitory inputs to the diversity of the firing patterns of IC neurons. The excitatory inputs are temporally diverse and create the basic temporal pattern, while the inhibitory inputs control the gain and, to a lesser extent, the firing pattern.

Recording sites

Our recordings are consistent with a previous study in the mouse ICC (Ehret & Moffat, 1985). They reported that most IC neurons had a first spike latency shorter than 20 ms, while some neurons had a latency longer than

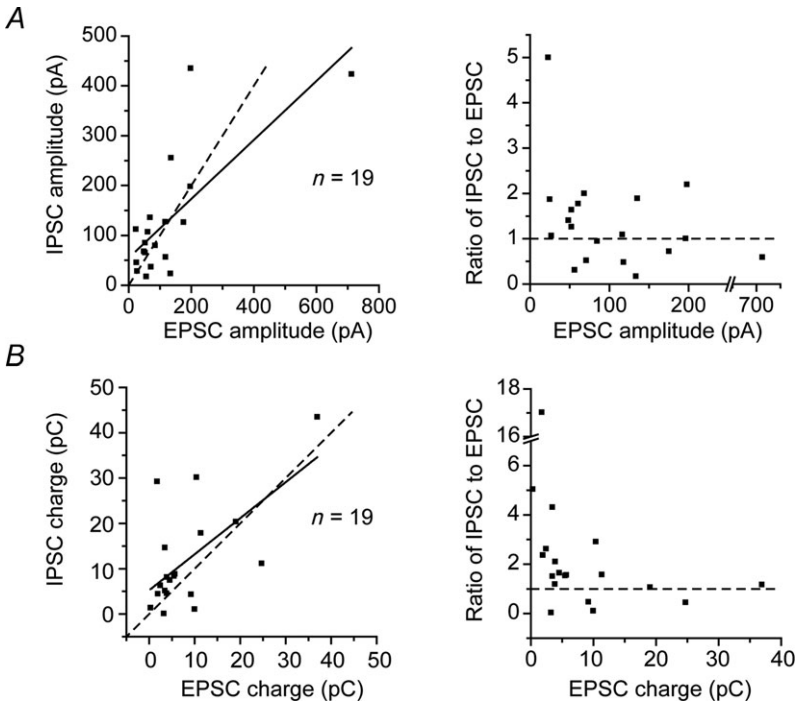

Figure 5. Size parameters of seEPSCs and seIPSCs recorded from the same neuron were positively correlated
The peak amplitude (*A*) and charge transfer (*B*) for seEPSCs and seIPSCs recorded from the same neuron. The upper left panels show the seEPSCs plotted against the seIPSCs. Dotted lines are lines of unity. The upper right panels show the seIPSC/seEPSC ratio plotted against the seEPSCs. Dotted lines indicate the level of 1. The black lines in the left panels show the linear fit. *A*, $y = 54.93 + 0.59x$; *B*, $y = 5.24 + 0.80x$.

50 ms. A typical first-spike latency of 10–20 ms (centred at approximately 12 ms; data not shown) is also seen in our own laboratory in extracellular recordings in the mouse ICC. Those recordings used the same 5 ms rise time for the acoustic stimulus used here. These values of spike latencies were close to the current onset values in this study. A recent *in vivo* whole-cell study in the mouse IC reported that the latency of tone-evoked EPSPs was approximately 10 ms when using a 3 ms stimulus rise time (Tan & Borst, 2007). The few milliseconds difference in latency between the studies may be due to the stimulus rise time difference, a series resistance error or a possible sampling error.

Intrinsic membrane properties

The intrinsic membrane properties may further modify the firing pattern as the IC neuron types differ in their expression of potassium currents (Sivaramakrishnan & Oliver, 2001; Ono *et al.* 2005; Tan *et al.* 2007). The

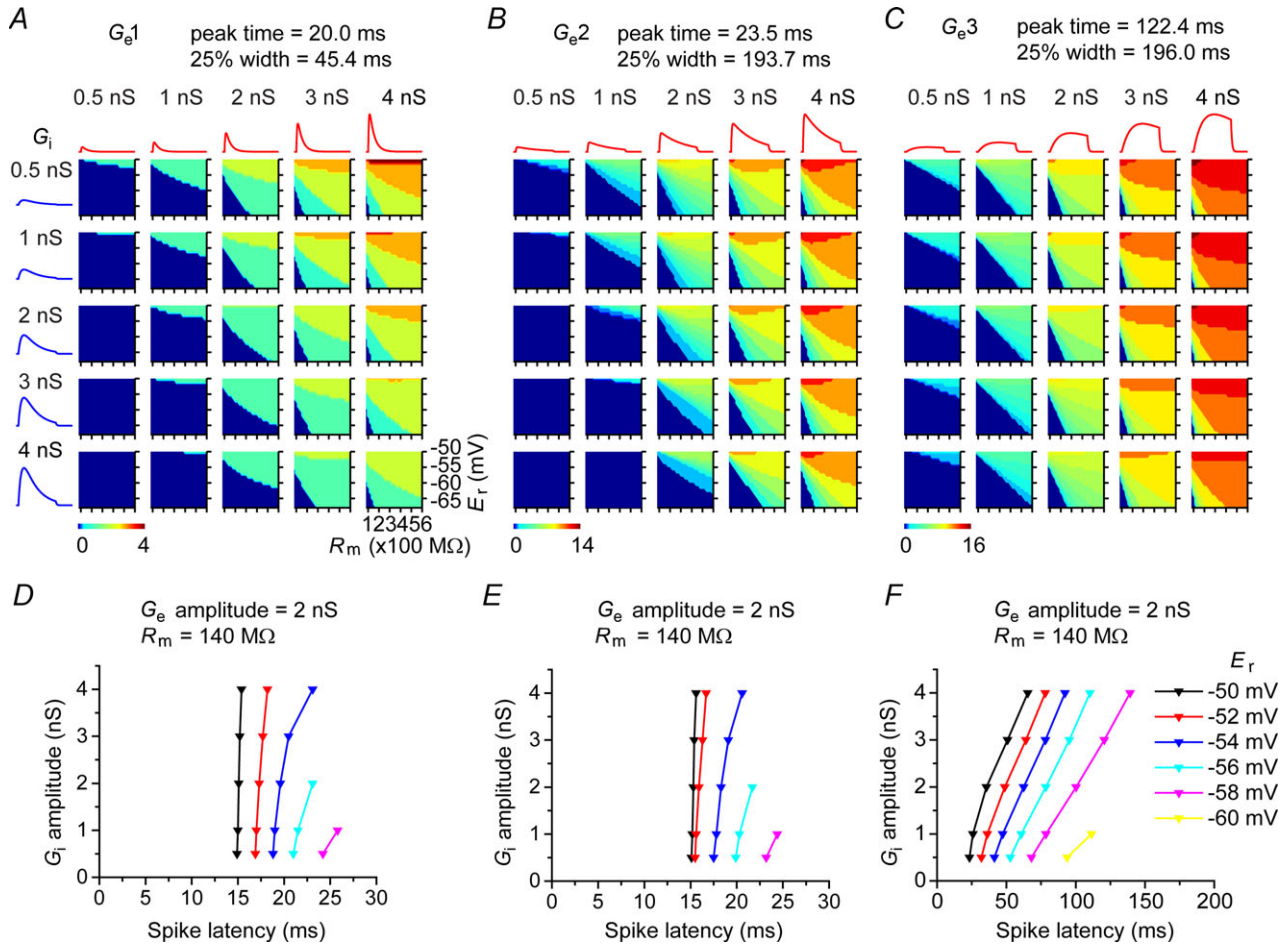

Figure 6. The integrate-and-fire model predicts the firing rate and latency based on the shape and amplitude of excitatory conductances, amplitude of inhibitory conductance and intrinsic membrane properties

A–C, three excitatory conductance models were used (*A*, G_e1, transient; *B*, G_e2, transient-sustained; *C*, G_e3, build-up). For each G_e pattern, the firing was stronger as R_m and E_r increased. With low R_m and E_r, the model frequently failed to fire. Each pseudocolour map shows the predicted firing to the combinations of G_e and G_i as membrane resistance (R_m) and resting potential (E_r) were varied. The colours indicate the number of action potentials. Inhibitory conductance (G_i) was varied in amplitude but not temporal pattern. A standard inhibitory conductance model (G_i) was used that was close to the mean values of recorded sIPSCs (peak time 42 ms, 25% width 140.1 ms). The red (upper) and blue (left) traces show the shapes of G_e and G_i, respectively. *D–F*, spike latency was found to be strongly dependent on E_r except in neurons with build-up excitation. The first spike latency for G_e (*D*, G_e1; *E*, G_e2; *F*, G_e3) is less affected by the G_i amplitude than it is by differences in E_r. The G_e amplitude was set at 2 nS, which was close to the mean amplitude of the recorded excitatory evoked conductances (1.65 ± 0.38 nS, $n = 28$). R_m was set at 140 MΩ, a value considered to be typical in mouse IC neurons (Geis & Borst, 2013). The latency was longer when E_r was lower (*D–F*).

Table 1. The parameters of G_e models

	Peak time (ms)	25% width (ms)	s	τ_1 (ms)	τ_2 (ms)	τ_3 (ms)
G_e1	20.0	45.4	1	4	25	5
G_e2	23.5	193.7	1	3	130	5
G_e3	122.4	196.0	1	63	300	5

interplay of synaptic and intrinsic factors surely shapes the final neural response (Tan & Borst, 2007). A number of voltage-gated and Ca^{2+}-activated currents may substantially influence the firing patterns in some IC neurons, although the intrinsic firing pattern does not appear to predict the sound-evoked firing pattern (Tan & Borst, 2007).

Our model did not include these conductances, but it may reasonably mimic the firing of many IC neurons with the regular-sustained firing and the invariant membrane resistance to the membrane potentials, which were reported to represent a large proportion of IC neurons studied *in vitro* (Peruzzi *et al.* 2000; Sivaramakrishnan & Oliver, 2001; Ono *et al.* 2005) and *in vivo* (Tan *et al.* 2007). These studies were done in young pups or young adult mice. Although developmental change in membrane resistance and firing were not reported in young adult mice between 3 and 5 weeks (Tan *et al.* 2007), it remains unknown if there are changes in intrinsic membrane properties in older animals.

Our model did show that R_m and E_r were critical factors in the firing rate, consistent with previous studies (Kuba *et al.* 2002; Yamada *et al.* 2005; Geis & Borst, 2009; Kuo & Wu, 2012). Since firing often failed with

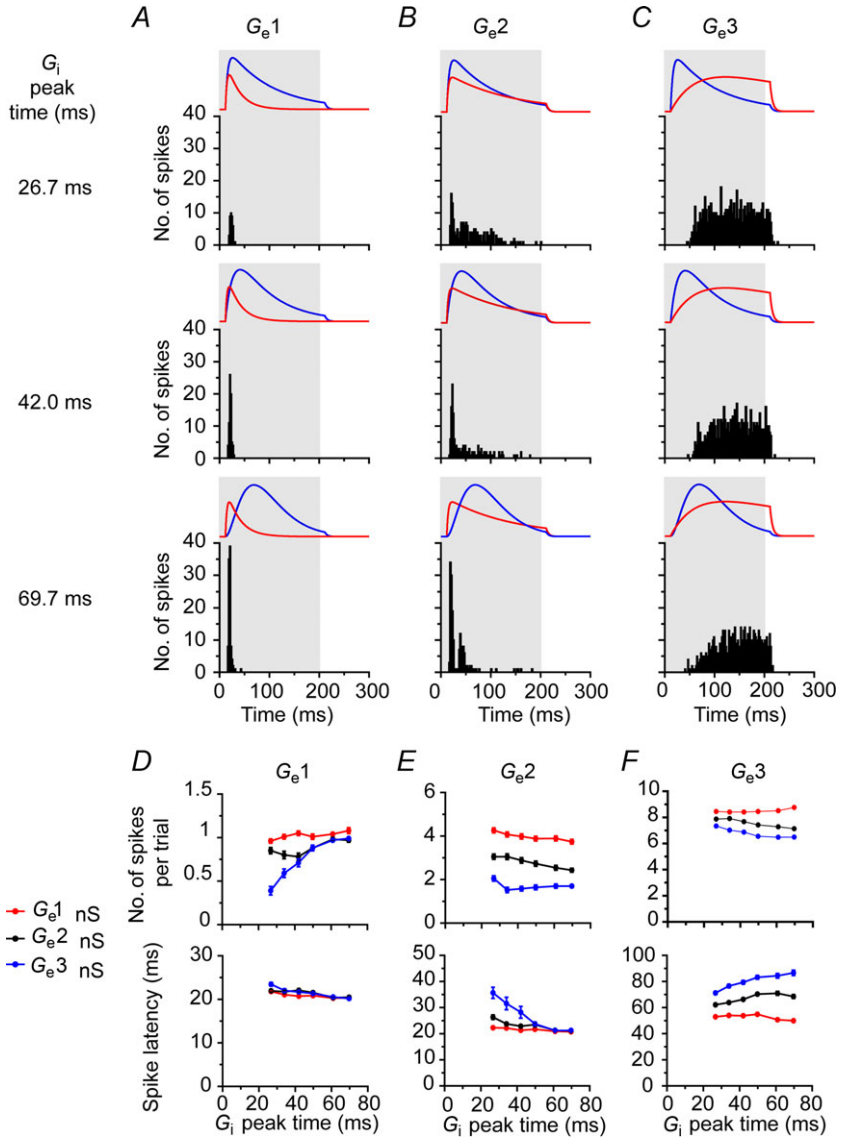

Figure 7. The peak time of the inhibitory conductance can change the spike rate and latency of the neurons
A–C, PSTHs showing the spike pattern predicted from three different G_e patterns, each 2 nS, and three different G_i peak times with a G_i of 3 nS. Note that the peak time of the inhibitory conductance can change the PSTH pattern of the neurons with early-peaked sustained EPSCs but not of the neurons with transient and build-up neurons. The red and blue traces above each PSTH indicate the G_e and G_i used to generate the responses, respectively. *A* and *D*, G_e1. *B* and *E*, G_e2. *C* and *F*, G_e3. *D–F*, the number of spikes per trial (upper) and the spike latency (lower) are plotted against the G_i peak time for three different sizes of G_i (1 nS red, 2 nS black, 3 nS blue).

Table 2. The parameters of G_i models with different peaks

Peak time (ms)	25% width (ms)	s	τ_1 (ms)	τ_2 (ms)	τ_3 (ms)
26.7	140.2	1	5	88	5
34.1	140.3	1	10	80	5
42.0	140.1	1	20	69	5
49.8	140.0	1	70	50	5
60.9	140.3	2	35	53	5
69.7	140.8	2	700	30	5

low R_m and E_r values and small excitatory inputs, this suggested that some neurons in our recordings might fail to fire in response to tones, a finding consistent with other whole-cell recordings *in vivo* (Tan & Borst, 2007; Xie *et al.* 2007).

What mechanisms generate seEPSCs and seIPSCs with different time courses?

The geometry and distribution of the synaptic terminals may influence the temporal character of the synaptic response profoundly. A calyx-type synapse is absent in the IC, where most ICC neurons have disc-shaped dendrites that parallel the layered afferent axons, thus creating the fibro-dendritic laminae of the ICC (Oliver & Morest, 1984). In comparison to the calyx, a single afferent axon makes repeated synaptic connections with the same neuron at different points along the dendrite; this behaviour would result in a less synchronised synaptic

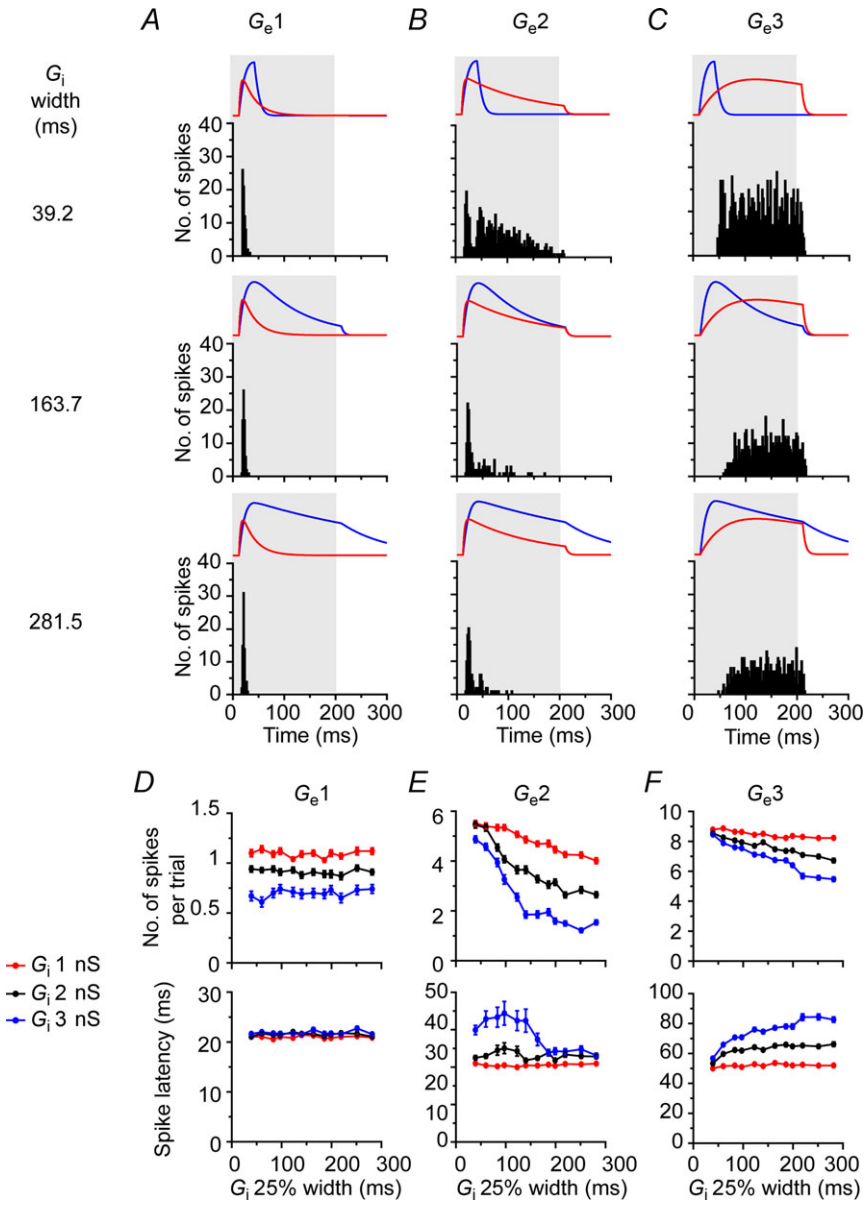

Figure 8. The duration of inhibitory conductance (G_i 25% width) changes the temporal pattern, firing rate, and latency of the early-peaked sustained neurons with more modest changes in the firing rate and latency of build-up neurons
Details are the same as in Fig. 7.

Table 3. The parameters of G_i models with different durations

Peak time (ms)	25% width (ms)	s	τ_1 (ms)	τ_2 (ms)	τ_3 (ms)
42.0	39.2	5	500	4	5
42.0	60.1	4	54	10	5
42.0	83.2	3	16	30	5
42.0	97.1	2	18	39	5
42.0	122.8	2	13	60	5
42.0	140.1	1	20	69	5
42.0	163.7	1	16	88	5
42.0	185.7	1	14	105	5
42.0	199.0	1	12	133	10
42.0	219.2	1	10	189	40
42.0	251.3	1	9	240	75
42.0	281.5	1	8	332	94

input. Moreover, the axon also will synapse on many other neurons within the same fibro-dendritic lamina. In this type of synaptic organisation, groups of axons with similar frequency tuning from the same source travel together within the same layer. The laminar geometry allows a few axons from the same source to dominate the inputs to a single neuron (Oliver, 2005; Loftus *et al.* 2010). Nevertheless, the asynchronous inputs would tend to blur the typical firing patterns from ascending sources such as the regular 'chopping' firing patterns of cochlear nucleus and lateral superior olivary neurons.

Cellular compartments that differ in synaptic density suggest a second type of synaptic organisation in IC neurons. For example, large GABAergic neurons have very dense glutamatergic synapses on the neuronal somata (Ito *et al.* 2009) that are not seen on other IC neurons. These inputs may converge from adjacent laminae and multiple sources (Ito & Oliver, 2012). An adequate acoustic stimulus may produce a more synchronised coincident activation of many of these axosomatic excitatory synapses on a large GABA neuron and create a powerful transient seEPSC.

The source of the presynaptic terminals may be a major factor in the temporal properties of the integrated synaptic response. The seEPSCs in the IC with diverse time courses match the early-peaking transient, sustained or build-up firing patterns observed in IC neurons with extracellular recordings (Ehret & Moffat, 1985; Rees *et al.* 1997). The anatomy of the laminar organisation in the ICC shows that many axons with similar BF and from the same source may terminate on the same

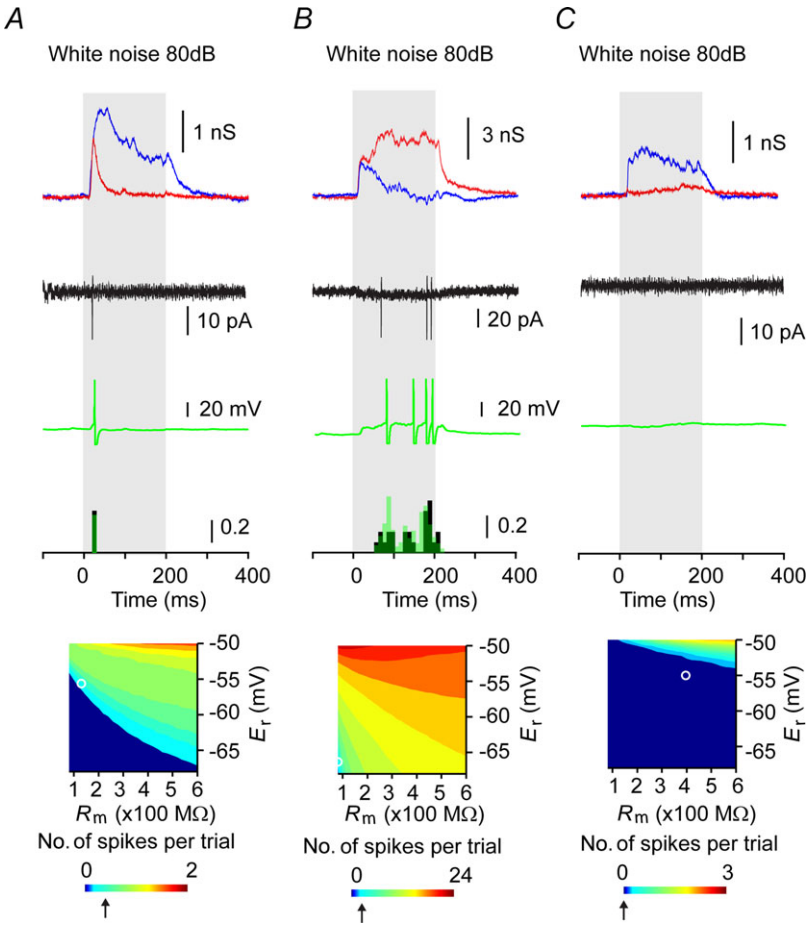

Figure 9. The integrate-and-fire model using recorded synaptic currents predicts the firing pattern obtained from the recorded cell in cell-attached mode
A–C, the comparison between the sound-evoked extracellular recordings and the predicted responses of the model. In these recordings, 80 dB SPL white noise (10–50 kHz) was used. Each figure consists of averaged synaptic responses obtained in whole-cell mode (top), a recording of spikes obtained in cell-attached mode (second row, black), a spike pattern predicted by the model (third row, green), PSTHs of recorded and modelled responses (fourth row) and the pseudocoloured map of the model response (bottom). In these figures, sound-evoked PSC traces have been converted into conductances. Red and blue traces are excitatory and inhibitory conductances, respectively. Pseudocoloured maps were constructed by systematically calculating the modelled responses to the recorded conductances at different R_m and E_r. Colour bars indicate the number of spikes per trial of the model responses. The arrows under the colour bars indicate the levels of recorded responses. White circles in the pseudocoloured maps indicate the points of R_m and E_r chosen for prediction.

neurons and the response of those postsynaptic neurons may resemble the source of the input. Glutamatergic neurons with different firing patterns project from the auditory brainstem to the IC (Ito & Oliver, 2010). The fusiform neurons in the dorsal cochlear nucleus project to ICC and have a build-up response (Rhode & Smith, 1986) that strongly resembles our build-up seEPSC. Our early-peaking, sustained-adapting seEPSC is the most ubiquitous and resembles a variety of brainstem neurons with projections to ICC, including the sustained-chopper of the ventral cochlear nucleus and the sustained response with onset in the lateral superior olive (Guinan *et al.* 1972*a*,*b*; Tsuchitani, 1977). This is the pattern most likely to be modified by the seIPSC and is unlikely to be an exact replica of the inputs in any case. Our early-peaking, transient seEPSCs most resemble the onset response of the octopus in the ventral cochlear nucleus (Rhode *et al.* 1983); however, because that cell does not project directly to the IC, the transient input is difficult to identify, although it may be a heavily filtered multi-spike transient response.

The onset-sustained and offset seIPSCs may arise from different sources. Most sources of GABAergic and glycinergic neurons that project to the IC are reported to have a strong onset component with a sustained-adapting post-stimulus firing pattern (Guinan *et al.* 1972*a*,*b*; Tsuchitani, 1977; Bajo *et al.* 1998; Kelly *et al.* 1998). This pattern is consistent with the less variable rapid rise and slow decay of our seIPSCs. However, the offset response of some seIPSCs resembles the offset responses in the superior periolivary nuclei, whose projections include the IC (Kulesza *et al.* 2003; Saldana *et al.* 2009).

The neurotransmitter receptor kinetics in the IC may also shape the temporal integration of presynaptic inputs. All IC neurons probably have AMPA and NMDA receptors (Zhang & Kelly, 2001; Wu *et al.* 2004; Sivaramakrishnan & Oliver, 2006; Sanchez *et al.* 2007; Malmierca & Hackett, 2010), GABA-A receptors and often glycine receptors (Park & Pollak, 1994; Sivaramakrishnan *et al.* 2004; Wu *et al.* 2004; Merchan *et al.* 2005; Nataraj & Wenstrup, 2005, 2006; Sanchez *et al.* 2008). The seEPSCs or seIPSCs with dissimilar temporal properties may be related to receptors with differences in subunit composition and kinetics. For example, it is not clear what proportion of the seEPSC here is due to the NMDA current and how much the NMDA component contributes to the temporal properties of different neuron types *in vivo*. In the IC, the NMDA channel may activate near the resting potential (Sivaramakrishnan & Oliver, 2006; Sanchez *et al.* 2007), but our recordings may underestimate the normal NMDA current. A second example is that large, medium and small neurons in the IC have different combinations of GABA-A receptor subunits (Shiraishi *et al.* 2001). This difference could also lead to seIPSCs with different kinetics in different neuron types.

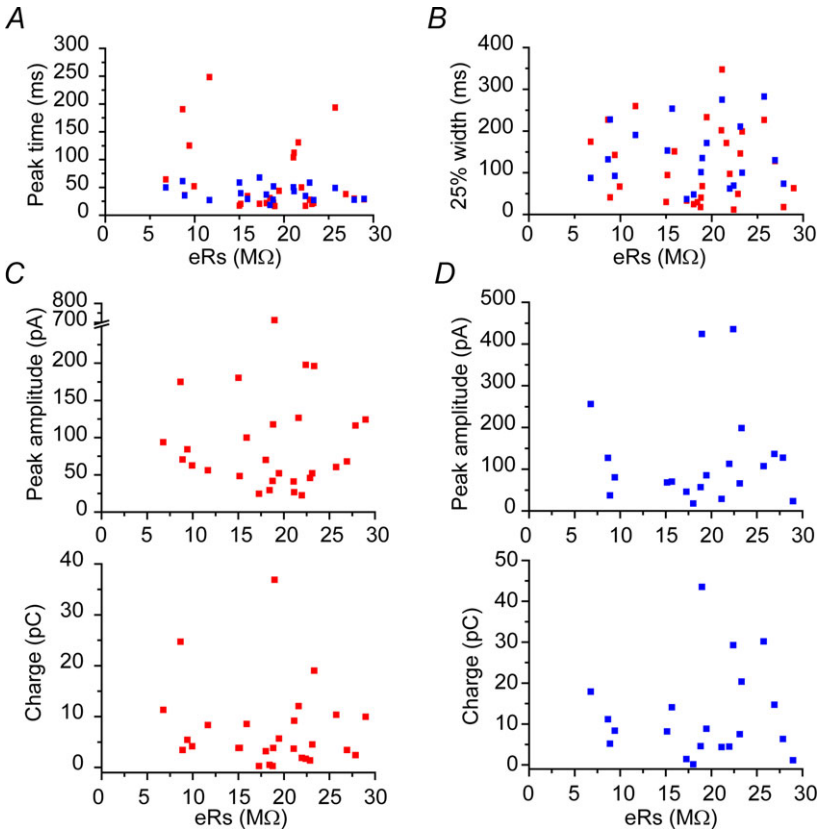

Figure 10. There was no correlation between the series resistance and the temporal parameters and size of sound-evoked synaptic inputs
A and *B*, peak times (*A*) and the 25% widths (*B*) of seEPSCs (red) and seIPSCs (blue) plotted against the effective series resistance (eRs). The averaged peak and width values across responses at different sound intensities were plotted. *C*, the size of seEPSCs calculated from the maximum responses of each neuron to monaural contralateral stimuli. Upper panel, peak amplitude; lower panel, charge transfer. The correlation coefficient was 0.11 between eRs and peak amplitude ($P = 0.60$), and −0.072 between eRs and charge transfer ($P = 0.74$). *D*, the size of seIPSCs. Upper panel, peak amplitude; lower panel, charge transfer. The correlation coefficient was 0.24 between eRs and peak amplitude ($P = 0.42$), and 0.10 between eRs and charge transfer ($P = 0.73$).

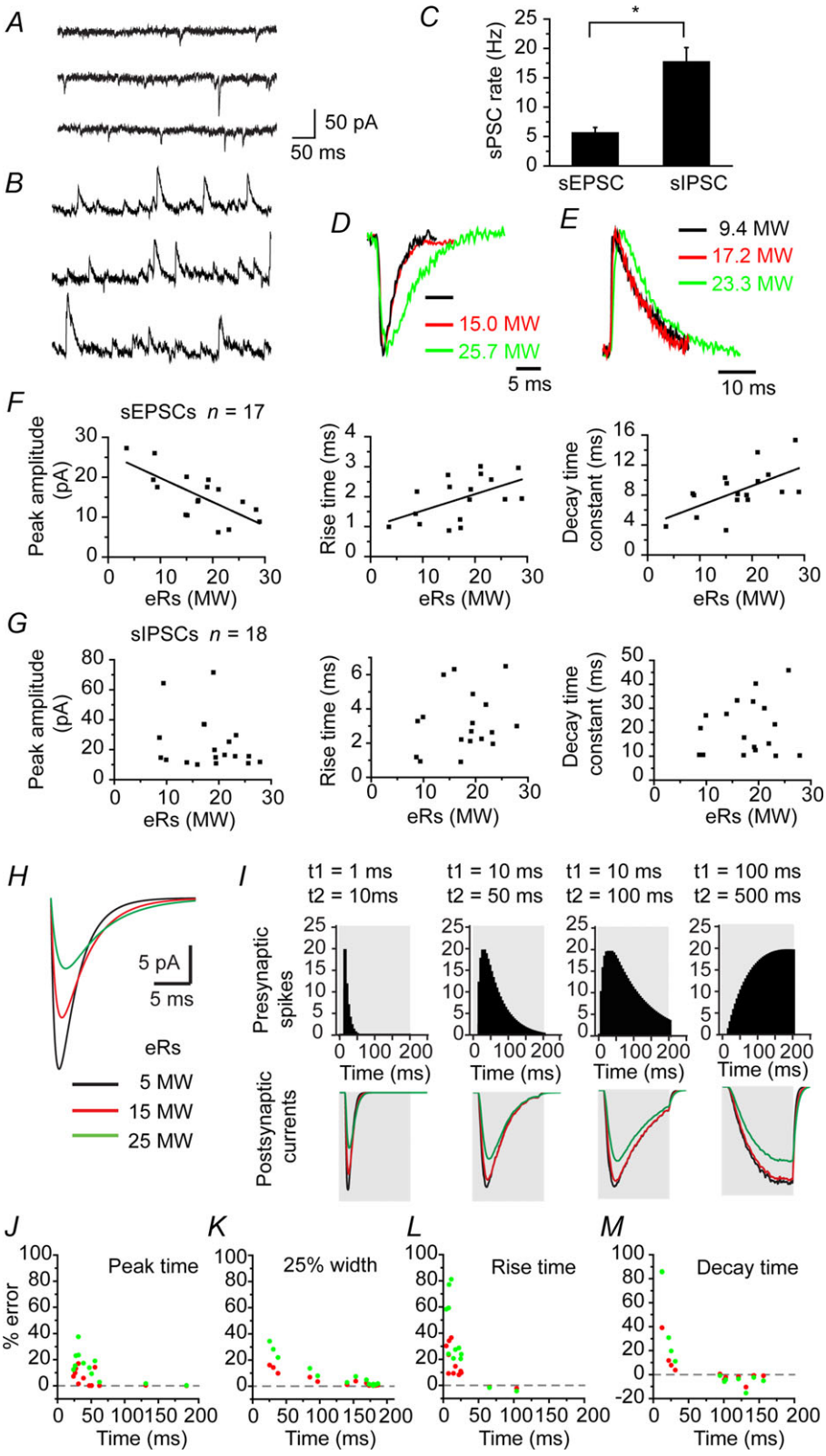

Figure 11. The model to estimate series resistance errors in sound-evoked responses shows that the uncompensated series resistance cannot explain seEPSCs of different shape, but it may make the size of synaptic currents smaller and the kinetics slower

A and *B*, examples of unaveraged spontaneous synaptic inputs recorded from different neurons (*A*, sEPSCs; *B*, sIPSCs). *C*, the frequency of sIPSCs (17.7 ± 2.4 Hz, $n = 19$) was significantly higher than that of sEPSCs

Functional consequences of diversity in seEPSCs and seIPSCs

The present data offer several new insights into the generation of firing patterns in the IC. The long duration of the synaptic currents may be important for the integration of sound-evoked activity in the IC. Unlike lower auditory centres, IC neurons have long membrane time constants and cannot phase lock to individual cycles of the stimulus; this feature, plus the asynchronous inputs, will result in a summation of individual synaptic events over time. Previous intracellular studies have shown sustained EPSPs in IC neurons that drive trains of action potentials in response to sound (Kuwada *et al.* 1997; Tan & Borst, 2007; Geis & Borst, 2009). Our findings demonstrate the synaptic currents that must underlie these potentials.

The tremendous variability in the peak time and duration of the seEPSCs usually shapes the overall time course of firing. Variable excitatory patterns were not reported in the previous studies *in vivo*, perhaps because the relatively brief acoustic stimuli used in those studies did not permit the observation and analysis of long-duration synaptic currents (Gittelman & Li, 2011; Gittelman *et al.* 2012; Li & Pollak, 2013).

Although the peak timing of seEPSCs and seIPSCs are not correlated and might be paired randomly, reproducible patterns occur due to differences in the variability of the excitatory and inhibitory peak times. The shortest latency, early-peaking, transient seEPSC usually precedes the seIPSC, while the late-peaking seEPSC follows the seIPSC. This reflects the typical peak timing of these currents and the relatively large variance in seEPSC peak times compared to the less variant seIPSC times. In the case of transient seEPSCs, the later seIPSCs may improve the accuracy of onset firing and avoid reducing the firing probability. In the auditory cortex, the seIPSC following the seEPSC was shown to reduce the temporal jittering of the onset firing (Wehr & Zador, 2003). In the case of delayed build-up seEPSCs, leading inhibition has been proposed as a key mechanism for duration tuning in the IC (Faure *et al.* 2003). Our data support this relationship. Since the sources of excitatory and the inhibitory synaptic currents in IC are independent and not necessarily driven by the same input, a variety of combinations is expected. However, all possible inputs to IC are not available to every IC neuron (Loftus *et al.* 2010), so the combination is from a restricted set of inputs.

The early-peaked sustained neuron may have the most modifiable firing pattern. The final integrated sound-evoked response of the neuron is a product of the combination of the asymmetrical excitatory and inhibitory inputs. The duration, size and peak latency of the inhibitory conductance could alter the firing pattern of early-peaked sustained cells. This effect was less evident for transient and buildup neurons. Previous studies on bats showed that the relative size and time course of the seIPSCs are critical in controlling the gain of the responses to frequency-modulated sweeps (Gittelman *et al.* 2009; Gittelman & Pollak, 2011). Our study demonstrates that seIPSCs can also control the shape of the firing pattern.

The inhibitory response to sound offset appears to be one temporal area where the integration of synaptic currents is lacking. Neurons with offset seIPSCs may be more common than neurons with EPSCs at sound offset (Kasai *et al.* 2012). The offset IPSCs may help the IC neurons to code the sound termination, by increasing the contrast of the firing probability before and after the sound ceases. In some cases, the pairing may have other functional significance, such as when a build-up seEPSC is paired with an offset$^+$ seIPSC. If

(5.6 ± 0.94 Hz, $n = 26$, $P < 0.001$, Wilcoxon signed-rank test). *D* and *E*, comparison of the time courses of sEPSCs (*D*) and sIPSCs (*E*) with different series resistance. The eRs of each trace is indicated. The trace used was the sPSCs with the fastest kinetics among the neurons with eRs = 0–10 MΩ (black), eRs = 10–20 MΩ (red) and eRs = 20–30 MΩ (green). The spontaneous events were averaged (>20) and the amplitudes were normalized. *F*, in sEPSCs, the parameters were strongly correlated with eRs. The absolute value of peak amplitude decreased as the series resistance increased (left, $R = -0.71$, $P = 0.0015$). In contrast, the rise time and the decay time constants increased as series resistance became higher (centre, the rise time, $R = 0.53$, $P = 0.028$; right, the decay time, $R = 0.61$, $P = 0.009$). Black lines show the linear fit. Left, $y = 25.81–0.60x$; middle, $y = 0.99 + 0.055x$; right, $y = 3.96 + 0.26x$. *G*, The parameters of sIPSCs were not well correlated with eRs (left, amplitude, $R = -0.24$, $P = 0.33$; centre, rise time, $R = 0.20$, $P = 0.42$; right, decay time, $R = 0.14$, $P = 0.58$), *H*, unitary EPSCs modelled with different series resistances. Their sizes, rise times and decay time constants were estimated from the fitting lines in *F*. Black, red and green traces represent the unitary response with eRs of 5, 15 and 25 MΩ, respectively. *I*, the sound-evoked responses (lower panels) were modelled by convolving the unitary responses and the PSTH of the presynaptic inputs (upper panels). The τ_1 and τ_2 used to generate the PSTH (see Methods) are above each panel. Black, red and green traces represent the modelled sound-evoked responses with eRs of 5, 15 and 25 MΩ, respectively. The grey boxes in the lower panels indicate the duration of the 200 ms sound. The height of the grey box indicates 250 pA in the left panel and 400 pA in other panels. *J–M*, the series resistance errors of the time course of the modelled sound-evoked responses are smaller in peak time and half width than in 10–90% rise time and decay time. Note that the error becomes smaller when the response time course becomes slower. *J*, peak time. *K*, 25% width. *L*, 10–90% rise time. *M*, 10–90% decay time. The percenatge error was plotted against the value of the response with the eRs of 5 MΩ.

a neuron with a build-up seEPSC has both a leading seIPSC and an offset seIPSC, it will lend itself particularly well to duration tuning (Faure *et al.* 2003). Both sustained and build-up synaptic inputs are appropriate to code for longer duration communication sounds, whereas excitatory transient onset and inhibitory offset currents may extract the beginning and the end of the sound, respectively (Kuwada & Batra, 1999; Kasai *et al.* 2012).

References

Acuna-Goycolea C, Tamamaki N, Yanagawa Y, Obata K & van den Pol AN (2005). Mechanisms of neuropeptide Y, peptide YY, and pancreatic polypeptide inhibition of identified green fluorescent protein-expressing GABA neurons in the hypothalamic neuroendocrine arcuate nucleus. *J Neurosci* **25**, 7406–7419.

Bajo VM, Villa AE, de Ribaupierre F & Rouiller EM (1998). Discharge properties of single neurons in the dorsal nucleus of the lateral lemniscus of the rat. *Brain Res Bull* **47**, 595–610.

Barker JL & Harrison NL (1988). Outward rectification of inhibitory postsynaptic currents in cultured rat hippocampal neurones. *J Physiol* **403**, 41–55.

Borst JG & Sakmann B (1996). Calcium influx and transmitter release in a fast CNS synapse. *Nature* **383**, 431–434.

Borst JG & Soria van Hoeve J (2012). The calyx of held synapse: from model synapse to auditory relay. *Annu Rev Physiol* **74**, 199–224.

Brand A, Urban R & Grothe B (2000). Duration tuning in the mouse auditory midbrain. *J Neurophysiol* **84**, 1790–1799.

Caspary DM, Raza A, Lawhorn Armour BA, Pippin J & Arneric SP (1990). Immunocytochemical and neurochemical evidence for age-related loss of GABA in the inferior colliculus: implications for neural presbycusis. *J Neurosci* **10**, 2363–2372.

Ehret G (1997). *The Auditory Midbrain, a 'Shunting Yard' of Acoustical Information Processing*. Oxford University Press, New York.

Ehret G & Moffat AJM (1985). Inferior colliculus of the house mouse II. Single unit responses to tones, noise and tone-noise combinations as a function of sound intensity. *J Comp Physiol A* **156**, 619–635.

Faure PA, Fremouw T, Casseday JH & Covey E (2003). Temporal masking reveals properties of sound-evoked inhibition in duration-tuned neurons of the inferior colliculus. *J Neurosci* **23**, 3052–3065.

Gardner SM, Trussell LO & Oertel D (1999). Time course and permeation of synaptic AMPA receptors in cochlear nuclear neurons correlate with input. *J Neurosci* **19**, 8721–8729.

Geis HR & Borst JG (2009). Intracellular responses of neurons in the mouse inferior colliculus to sinusoidal amplitude-modulated tones. *J Neurophysiol* **101**, 2002–2016.

Geis HR & Borst JG (2013). Large GABAergic neurons form a distinct subclass within the mouse dorsal cortex of the inferior colliculus with respect to intrinsic properties, synaptic inputs, sound responses, and projections. *J Comp Neurol* **521**, 189–202.

Gittelman JX & Li N (2011). FM velocity selectivity in the inferior colliculus is inherited from velocity-selective inputs and enhanced by spike threshold. *J Neurophysiol* **106**, 2399–2414.

Gittelman JX, Li N & Pollak GD (2009). Mechanisms underlying directional selectivity for frequency-modulated sweeps in the inferior colliculus revealed by in vivo whole-cell recordings. *J Neurosci* **29**, 13030–13041.

Gittelman JX & Pollak GD (2011). It's about time: how input timing is used and not used to create emergent properties in the auditory system. *J Neurosci* **31**, 2576–2583.

Gittelman JX, Wang L, Colburn HS & Pollak GD (2012). Inhibition shapes response selectivity in the inferior colliculus by gain modulation. *Front Neural Circuits* **6**, 67.

Golding NL & Oertel D (2012). Synaptic integration in dendrites: exceptional need for speed. *J Physiol* **590**, 5563–5569.

Guinan JJ, Guinan SS & Norris BE (1972*a*). Single auditory units in the superior olivary complex I: Responses to sounds and classifications based on physiological properties. *Int J Neurosci* **4**, 101–120.

Guinan JJ, Norris BE & Guinan SS (1972*b*). Single auditory units in the superior olivary complex II: Locations of unit categories and tonotopic organization. *Int J Neurosci* **4**, 147–166.

Hodgkin AL & Katz B (1949). The effect of sodium ions on the electrical activity of giant axon of the squid. *J Physiol* **108**, 37–77.

Ito T, Bishop DC & Oliver DL (2009). Two classes of GABAergic neurons in the inferior colliculus. *J Neurosci* **29**, 13860–13869.

Ito T & Oliver DL (2010). Origins of glutamatergic terminals in the inferior colliculus identified by retrograde transport and expression of VGLUT1 and VGLUT2 genes. *Front Neuroanat* **4**, 135.

Ito T & Oliver DL (2012). The basic circuit of the IC: tectothalamic neurons with different patterns of synaptic organization send different messages to the thalamus. *Front Neural Circuits* **6**, 48.

Kasai M, Ono M & Ohmori H (2012). Distinct neural firing mechanisms to tonal stimuli offset in the inferior colliculus of mice in vivo. *Neurosci Res* **73**, 224–237.

Kelly JB, Buckthought AD & Kidd SA (1998). Monaural and binaural response properties of single neurons in the rat's dorsal nucleus of the lateral lemniscus. *Hear Res* **122**, 25–40.

Kuba H, Koyano K & Ohmori H (2002). Development of membrane conductance improves coincidence detection in the nucleus laminaris of the chicken. *J Physiol* **540**, 529–542.

Kuba H, Yamada R, Fukui I & Ohmori H (2005). Tonotopic specialization of auditory coincidence detection in nucleus laminaris of the chick. *J Neurosci* **25**, 1924–1934.

Kulesza RJ Jr, Spirou GA & Berrebi AS (2003). Physiological response properties of neurons in the superior paraolivary nucleus of the rat. *J Neurophysiol* **89**, 2299–2312.

Kuo RI & Wu GK (2012). The generation of direction selectivity in the auditory system. *Neuron* **73**, 1016–1027.

Kuwada S & Batra R (1999). Coding of sound envelopes by inhibitory rebound in neurons of the superior olivary complex in the unanesthetized rabbit. *J Neurosci* **19**, 2273–2287.

Kuwada S, Batra R, Yin TC, Oliver DL, Haberly LB & Stanford TR (1997). Intracellular recordings in response to monaural and binaural stimulation of neurons in the inferior colliculus of the cat. *J Neurosci* **17**, 7565–7581.

Li N & Pollak GD (2013). Circuits that innervate excitatory–inhibitory cells in the inferior colliculus obtained with in vivo whole cell recordings. *J Neurosci* **33**, 6367–6379.

Loftus WC, Bishop DC & Oliver DL (2010). Differential patterns of inputs create functional zones in central nucleus of inferior colliculus. *J Neurosci* **30**, 13396–13408.

Malmierca MS & Hackett TA (2010). Structural organization of the ascending auditory pathway. In *The Oxford Handbook of Auditory Science: The Auditory Brain*, ed. Rees A & Palmer AR, pp. 9–42. Oxford University Press, Oxford.

Manis PB & Marx SO (1991). Outward currents in isolated ventral cochlear nucleus neurons. *J Neurosci* **11**, 2865–2880.

Margrie TW, Brecht M & Sakmann B (2002). In vivo, low-resistance, whole-cell recordings from neurons in the anaesthetized and awake mammalian brain. *Pflugers Arch* **444**, 491–498.

Mayer ML, Westbrook GL & Guthrie PB (1984). Voltage-dependent block by Mg^{2+} of NMDA responses in spinal cord neurones. *Nature* **309**, 261–263.

Merchan M, Aguilar LA, Lopez-Poveda EA & Malmierca MS (2005). The inferior colliculus of the rat: quantitative immunocytochemical study of GABA and glycine. *Neuroscience* **136**, 907–925.

Moroni M, Biro I, Giugliano M, Vijayan R, Biggin PC, Beato M & Sivilotti LG (2011). Chloride ions in the pore of glycine and GABA channels shape the time course and voltage dependence of agonist currents. *J Neurosci* **31**, 14095–14106.

Nataraj K & Wenstrup JJ (2005). Roles of inhibition in creating complex auditory responses in the inferior colliculus: facilitated combination-sensitive neurons. *J Neurophysiol* **93**, 3294–3312.

Nataraj K & Wenstrup JJ (2006). Roles of inhibition in complex auditory responses in the inferior colliculus: inhibited combination-sensitive neurons. *J Neurophysiol* **95**, 2179–2192.

Oliver DL (2005). Neuronal organization in the inferior colliculus. Chapter 2. In *The Inferior Colliculus*, ed. Winer JA & Schreiner CE, pp. 69–114. Springer, New York.

Oliver DL & Morest DK (1984). The central nucleus of the inferior colliculus in the cat. *J Comp Neurol* **222**, 237–264.

Ono M, Yanagawa Y & Koyano K (2005). GABAergic neurons in inferior colliculus of the GAD67-GFP knock-in mouse: electrophysiological and morphological properties. *Neurosci Res* **51**, 475–492.

Ozawa S, Kamiya H & Tsuzuki K (1998). Glutamate receptors in the mammalian central nervous system. *Prog Neurobiol* **54**, 581–618.

Park TJ & Pollak GD (1994). Azimuthal receptive fields are shaped by GABAergic inhibition in the inferior colliculus of the mustache bat. *J Neurophysiol* **72**, 1080–1102.

Peruzzi D, Sivaramakrishnan S & Oliver DL (2000). Identification of cell types in brain slices of the inferior colliculus. *Neuroscience* **101**, 403–416.

Rees A, Sarbaz A, Malmierca MS & Le Beau FE (1997). Regularity of firing of neurons in the inferior colliculus. *J Neurophysiol* **77**, 2945–2965.

Rhode WS & Greenberg S (1992). Physiology of the cochlear nuclei. In *The Mammalian Auditory Pathway: Neurophysiology*, 1st edn, ed. Popper AN & Fay RR, pp. 94–152. Springer-Verlag, NY.

Rhode WS, Oertel D & Smith PH (1983). Physiological response properties of cells labelled intracellularly with horseradish peroxidase in cat ventral cochlear nucleus. *J Comp Neurol* **213**, 448–463.

Rhode WS & Smith PH (1986). Physiological studies on neurons in the dorsal cochlear nucleus of cat. *J Neurophysiol* **56**, 287–307.

Rodriguez FA, Chen C, Read HL & Escabi MA (2010). Neural modulation tuning characteristics scale to efficiently encode natural sound statistics. *J Neurosci* **30**, 15969–15980.

Saldana E, Aparicio MA, Fuentes-Santamaria V & Berrebi AS (2009). Connections of the superior paraolivary nucleus of the rat: projections to the inferior colliculus. *Neuroscience* **163**, 372–387.

Sanchez JT, Gans D & Wenstrup JJ (2007). Contribution of NMDA and AMPA receptors to temporal patterning of auditory responses in the inferior colliculus. *J Neurosci* **27**, 1954–1963.

Sanchez JT, Gans D & Wenstrup JJ (2008). Glycinergic 'inhibition' mediates selective excitatory responses to combinations of sounds. *J Neurosci* **28**, 80–90.

Shiraishi S, Shiraishi Y, Oliver DL & Altschuler RA (2001). Expression of $GABA_A$ receptor subunits in the rat central nucleus of the inferior colliculus. *Brain Res Mol Brain Res* **96**, 122–132.

Sivaramakrishnan S & Oliver DL (2001). Distinct K currents result in physiologically distinct cell types in the inferior colliculus of the rat. *J Neurosci* **21**, 2861–2877.

Sivaramakrishnan S & Oliver DL (2006). Neuronal responses to lemniscal stimulation in laminar brain slices of the inferior colliculus. *J Assoc Res Otolaryngol* **7**, 1–14.

Sivaramakrishnan S, Sterbing-D'Angelo SJ, Filipovic B, D'Angelo WR, Oliver DL & Kuwada S (2004). $GABA_A$ synapses shape neuronal responses to sound intensity in the inferior colliculus. *J Neurosci* **24**, 5031–5043.

Sun YJ, Wu GK, Liu BH, Li P, Zhou M, Xiao Z, Tao HW & Zhang LI (2010). Fine-tuning of pre-balanced excitation and inhibition during auditory cortical development. *Nature* **465**, 927–931.

Tamamaki N, Yanagawa Y, Tomioka R, Miyazaki J, Obata K & Kaneko T (2003). Green fluorescent protein expression and colocalization with calretinin, parvalbumin, and somatostatin in the GAD67-GFP knock-in mouse. *J Comp Neurol* **467**, 60–79.

Tan ML & Borst JG (2007). Comparison of responses of neurons in the mouse inferior colliculus to current injections, tones of different durations, and sinusoidal amplitude-modulated tones. *J Neurophysiol* **98**, 454–466.

Tan ML, Theeuwes HP, Feenstra L & Borst JG (2007). Membrane properties and firing patterns of inferior colliculus neurons: an in vivo patch-clamp study in rodents. *J Neurophysiol* **98**, 443–453.

Tsuchitani C (1977). Functional organization of lateral cell groups of cat superior olivary complex. *J Neurophysiol* **40**, 296–318.

Urban GP & Willott JF (1979). Response properties of neurons in inferior colliculi of mice made susceptible to audiogenic seizures by acoustic priming. *Exp Neurol* **63**, 229–243.

Wehr M & Zador AM (2003). Balanced inhibition underlies tuning and sharpens spike timing in auditory cortex. *Nature* **426**, 442–446.

Williams SR & Mitchell SJ (2008). Direct measurement of somatic voltage clamp errors in central neurons. *Nat Neurosci* **11**, 790–798.

Wu SH, Ma CL & Kelly JB (2004). Contribution of AMPA, NMDA, and $GABA_A$ receptors to temporal pattern of postsynaptic responses in the inferior colliculus of the rat. *J Neurosci* **24**, 4625–4634.

Xie R, Gittelman JX & Pollak GD (2007). Rethinking tuning: in vivo whole-cell recordings of the inferior colliculus in awake bats. *J Neurosci* **27**, 9469–9481.

Xiong XR, Liang F, Li H, Mesik L, Zhang KK, Polley DB, Tao HW, Xiao Z & Zhang LI (2013). Interaural level difference-dependent gain control and synaptic scaling underlying binaural computation. *Neuron* **79**, 738–753.

Yamada R, Kuba H, Ishii TM & Ohmori H (2005). Hyperpolarization-activated cyclic nucleotide-gated cation channels regulate auditory coincidence detection in nucleus laminaris of the chick. *J Neurosci* **25**, 8867–8877.

Young ED & Oertel D (2010). Cochlear nucleus. In *Handbook of Brain Microcircuits*, ed. Shepherd GM, Grillner S, pp. 215–223. Oxford University Press, New York.

Zar JH (1998). *Biostatistical Analysis*. Prentice Hall, New Jersey.

Zhang H & Kelly JB (2001). AMPA and NMDA receptors regulate responses of neurons in the rat's inferior colliculus. *J Neurophysiol* **86**, 871–880.

Additional Information

Competing interests

None

Author contributions

M.O. conducted the experiments and analysed the data. M.O. and D.L.O. jointly conceived and designed the study and jointly wrote the paper. All authors approved the final version.

Funding

This project was funded by NIDCD grant R01 DC000189.

Acknowledgements

We thank Shigeyuki Kuwada, Srdjan D. Antic and Shobhana Sivaramakrishnan for their critical comments on the manuscript. We would also like to thank Shigeyuki Kuwada and Duck O. Kim for their technical help and advice.